0026-895X/11/8006-965–978
MOLECULAR PHARMACOLOGY
U.S. Government work not protected by U.S. copyright
Mol Pharmacol 80:965–978, 2011

Vol. 80, No. 6
71225/3722630
Printed in U.S.A.

2-Aminoethyl Methylphosphonate, a Potent and Rapidly Acting Antagonist of $GABA_A$-ρ1 Receptors

An Xie, Jun Yan, Lan Yue, Feng Feng, Fozia Mir, Heba Abdel-Halim, Mary Chebib, Guy C. Le Breton, Robert F. Standaert, Haohua Qian, and David R. Pepperberg

Lions of Illinois Eye Research Institute, Department of Ophthalmology and Visual Sciences, University of Illinois at Chicago, College of Medicine, Chicago, Illinois (A.X., L.Y., F.F., H.Q., D.R.P.); Biosciences Division, Oak Ridge National Laboratory, Oak Ridge, Tennessee (J.Y., R.F.S.); Chengdu Kanghong Pharmaceutical Co. Ltd., Sichuan, People's Republic of China (J.Y.); Department of Bioengineering, University of Illinois at Chicago, Chicago, Illinois (L.Y., D.R.P.); Department of Pharmacological Sciences, University of Illinois at Chicago, College of Medicine, Chicago, Illinois (F.M., G.C.L.); Faculty of Pharmacy, The University of Sydney, Sydney, Australia (H.A-H., M.C.); Department of Biochemistry and Cellular & Molecular Biology, University of Tennessee, Knoxville, Tennessee (R.F.S.); and National Eye Institute, National Institutes of Health, Bethesda, Maryland (H.Q.)

Received January 14, 2011; accepted August 2, 2011

ABSTRACT

2-Aminoethyl methylphosphonate (2-AEMP), an analog of GABA, has been found to exhibit antagonist activity at $GABA_A$-ρ1 (also known as ρ1 $GABA_C$) receptors. The present study was undertaken to elucidate 2-AEMP's action and to test the activities of 2-AEMP analogs. Whole-cell patch-clamp techniques were used to record membrane currents in neuroblastoma cells stably transfected with human $GABA_A$-ρ1 receptors. The action of 2-AEMP was compared with that of 1,2,5,6-tetrahydropyridin-4-yl methylphosphinic acid (TPMPA), a commonly used $GABA_A$-ρ1 antagonist. With 10 μM GABA, 2-AEMP's IC_{50} (18 μM) differed by less than 2.5-fold from that of TPMPA (7 μM), and results obtained were consistent with a primarily competitive mode of inhibition by 2-AEMP. Terminating the presentation of 2-AEMP or TPMPA in the presence of GABA produced a release from inhibition. However, the rate of inhibition release upon the termination of 2-AEMP considerably exceeded that determined with termination of TPMPA. Moreover, when presented at concentrations near their respective IC_{50} values, the preincubation period associated with 2-AEMP's onset of inhibition was much shorter than that for TPMPA. Analogs of 2-AEMP possessing a benzyl or *n*-butyl rather than a methyl substituent at the phosphorus atom, as well as analogs bearing a C-methyl substituent on the aminoethyl side chain, exhibited reduced potency relative to 2-AEMP. Of these analogs, only (*R*)-2-aminopropyl methylphosphonate significantly diminished the response to 10 μM GABA. Structure-activity relationships are discussed in the context of molecular modeling of ligand binding to the antagonist binding site of the $GABA_A$-ρ1 receptor.

Introduction

GABA (Fig. 1) is a major inhibitory neurotransmitter with three distinct types of postsynaptic receptors, $GABA_A$, $GABA_B$, and $GABA_A$-ρ (also known as $GABA_C$) (Olsen and Sieghart, 2009). The $GABA_A$-ρ receptor, a member of the family of cysteine-loop pentameric, ligand-gated ion channels, is distributed in the retina and elsewhere in the central nervous system (Qian and Dowling, 1993; Enz et al., 1995; Lukasiewicz, 2005). Native $GABA_A$-ρ receptors consist of a combination of ρ1, ρ2, and ρ3 subunits. However, ρ1 subunits can assemble to form functional homopentameric receptors, and the ρ1 receptor ($GABA_A$-ρ1) has been widely studied as a model system in both amphibian and mammalian expression systems (Chang and Weiss, 1999; Chebib, 2004; Sedelnikova et al., 2005; Song et al., 2005; Vu et al., 2005).

Insight into the physiology of $GABA_A$-ρ1 receptors has come from studies of 1,2,5,6-tetrahydropyridin-4-yl methylphosphinic acid (TPMPA), a phosphinic analog of GABA that was the first selective antagonist for $GABA_A$-ρ1 to be discovered (Murata et al., 1996; Ragozzino et al., 1996; Krehan et al., 2003; Chebib et al., 2007). 3-Aminopropyl methylphos-

This work was supported by the National Institutes of Health National Eye Institute [Grants EY016094, EY001792]; the National Institutes of Health National Heart, Lung, and Blood Institute [Grant HL024530]; the Daniel F. and Ada L. Rice Foundation; Hope for Vision; the Macular Degeneration Research Program of the American Health Assistance Foundation; the Arnold and Mabel Beckman Initiative for Macular Research; Research to Prevent Blindness; and the Laboratory Directed Research and Development Program of Oak Ridge National Laboratory, managed by UT-Battelle, LLC, for the United States Department of Energy.

Article, publication date, and citation information can be found at http://molpharm.aspetjournals.org.

doi:10.1124/mol.111.071225.

ABBREVIATIONS: TPMPA, 1,2,5,6-tetrahydropyridin-4-yl methylphosphinic acid; 2-AEMP, 2-aminoethyl methylphosphonate; 3-APMPA, 3-aminopropyl methylphosphinic acid; *s*-Bu, secondary butyl; Cbz, carbobenzyloxy; DCM, dichloromethane; DEAD, diethyl azodicarboxylate; DIPEA, *N*,*N*-diisopropylethylamine; THF, tetrahydrofuran; TLC, thin-layer chromatography; trityl, triphenylmethyl.

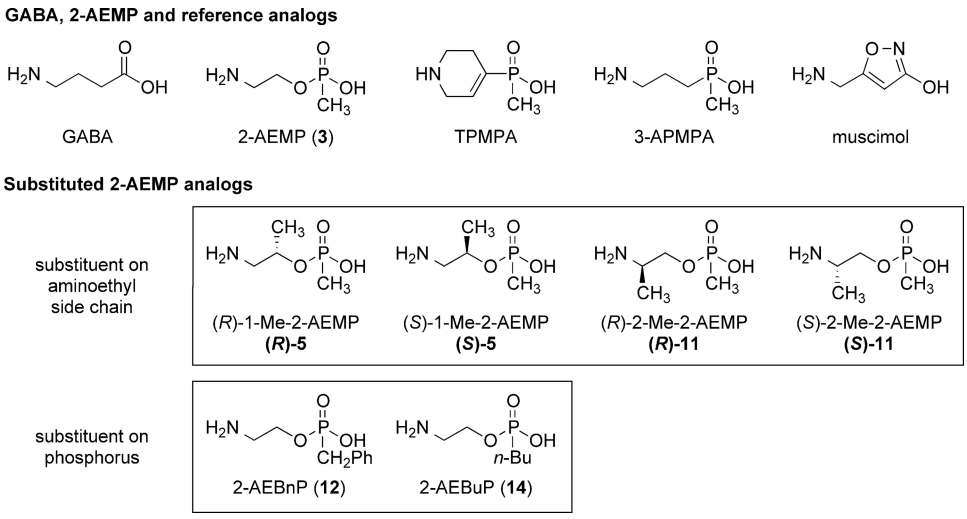

Fig. 1. Structures of GABA and analogs pertinent to the present study. 2-AEBnP, 2-aminoethyl benzylphosphonate; 2-AEBuP, 2-aminoethyl *n*-butylphosphonate.

phinic acid (3-APMPA), an acyclic phosphinic analog that is isosteric with GABA, is the most potent $GABA_A$-ρ1 antagonist known, but it is also a potent agonist of $GABA_B$ receptors (Howson et al., 1993; Froestl et al., 1995a,b). The tetrahydropyridyl ring of TPMPA is believed to impair binding to the $GABA_B$ receptor, accounting for its high $GABA_A$-ρ1 selectivity (Ragozzino et al., 1996).

Phosphonic acid analogs of GABA, unlike phosphinic analogs such as TPMPA and 3-APMPA, have not been investigated extensively. Cates et al. (1984) showed that 2-aminoethyl phenylphosphonate weakly inhibits the binding of [^{3}H]GABA to $GABA_A$ and $GABA_B$ receptors in rat brain. Overall however, phosphonic analogs of GABA are much less well characterized, and structure-activity relationships within this class are unknown. Chowdhury et al. (2007) have reported the synthesis of 2-aminoethyl methylphosphonic acid (2-AEMP) (Fig. 1) and described the antagonist activity of this compound at $GABA_A$-ρ1 receptors expressed in *Xenopus laevis* oocytes. 2-AEMP differs from 3-APMPA in possessing an oxygen atom rather than a methylene group bonded to the phosphorus atom at the position corresponding to carbon-2 of GABA.

The present study was undertaken with two main objectives. The first was to gain a better understanding of the action of 2-AEMP, the parent of the alkylphosphonate class of GABA analogs. In this article, we report electrophysiological experiments conducted with whole-cell patch clamp on $GABA_A$-ρ1 receptors stably expressed in a neuroblastoma cell line. Using this mammalian cell line, we also have performed competition binding experiments on $GABA_A$-ρ1-expressing whole cells, results of which we present here. The second objective was to determine whether substitution at any of the carbon atoms of 2-AEMP preserves significant activity of the compound at $GABA_A$-ρ1 receptors. This question is of interest for potential neurobiology applications in which a chain-derivatized form of this type of GABA analog could be tethered to an anchoring surface via, for instance, streptavidin (Saifuddin et al., 2003; Nehilla et al., 2004; Vu et al., 2005), to a nanoparticle (Gussin et al., 2006), or to the receptor itself (Volgraf et al., 2006; Numano et al., 2009). 2-AEMP derivatives are relatively easy to prepare, and the key building blocks, phosphonic acids and 2-aminoalcohols, are readily available. Accordingly, we have synthesized two new derivatives of 2-AEMP substituted at the *P*-methyl group and four new derivatives substituted at the methylene carbons of the aminoethyl group. We have assessed the potencies of these compounds as antagonists at $GABA_A$-ρ1 receptors and have interpreted the results in relation to a ligand-docking model for $GABA_A$-ρ1 that has been used by Abdel-Halim et al. (2008). This model, which was developed to screen for antagonists, was obtained by optimizing the fit (i.e., minimizing the interaction energy) of TPMPA with the receptor, using quantum mechanical and molecular mechanics calculations. Preliminary results of the electrophysiological experiments have been reported in abstract form (Xie et al., 2008, 2009).

Materials and Methods

The experiments were performed on stably transfected neuroblastoma cells (SHp5-ρ1 cells) expressing human $GABA_A$-ρ1 receptors (cell line kindly provided by Dr. David S. Weiss, University of Texas at San Antonio, San Antonio, TX). Control, nonexpressing neuroblastoma cells (SHSY5Y) were obtained from the American Type Culture Collection (Manassas, VA). Experiments were also conducted on oocytes obtained from *Xenopus laevis* frogs (Xenopus One, Ann Arbor, MI). All animal procedures adhered to institutional policies and to the Statement for the Use of Animals in Ophthalmic and Vision Research adopted by the Association for Research in Vision and Ophthalmology.

Synthesis of Test Compounds. All chemicals were purchased from commercial suppliers and used as received. Analytical thin-layer chromatography (TLC) was performed with plastic-backed TLC silica gel 60F hard-layer plates (Scientific Adsorbents, Atlanta, GA). TLC plates were visualized by staining with 5% (w/v) phosphomolybdic acid in ethanol or by UV shadowing (254 nm). Column chromatography was performed using silica gel (200–400 mesh size) and indicated eluents. NMR spectra were recorded at the indicated frequencies. Chemical shifts (δ) are reported in parts per million downfield from tetramethylsilane and were referenced to internal tetramethylsilane or to solvent peaks ($CHCl_3$, 7.26; $CDCl_3$, 77.0; CD_2HOD, 3.31; CD_3OD, 49.0).

2-(Triphenylmethylamino)ethanol (1). To a solution of ethanolamine (5.0 g, 81.9 mmol) in dichloromethane (DCM; 50 ml) was added triphenylmethyl (trityl) chloride (27.4 g, 98.3 mmol) and *N*,*N*-diisopropylethylamine (DIPEA; 21.4 ml, 123 mmol) at 0°C, and the stirred solution was allowed to warm to room temperature. The solution was stirred for 3 h and then washed with water (2 × 30 ml) and brine (20 ml). The organic layer was dried over Na_2SO_4 and concentrated to a clear oil. Purification by chromatography on silica

gel (EtOAc/hexanes, 1:2) afforded the product as a white solid (22.6 g, 91%). ^{1}H NMR (400 MHz, CD_3OD) δ 7.48 (6H, d, J = 7.6 Hz), 7.27 (6H, t, J = 7.4 Hz), 7.18 (3H, t, J = 7.3 Hz), 3.67 (2H, t, J = 5.6 Hz), 2.29 (2H, t, J = 5.6 Hz); ^{13}C NMR (100 MHz, CD_3OD) δ 146.9, 129.3, 128.1, 126.7, 70.9, 61.9, 45.9.

2-(Triphenylmethylamino)ethyl methylphosphonate (2). To a solution of triphenylphosphine (3.21 g, 12.2 mmol) in anhydrous THF (50 ml) at 0°C was added drop-wise diethyl azodicarboxylate (DEAD; 2.13 g, 12.2 mmol) followed by a solution of methylphosphonic acid (0.978 g, 10.2 mmol) in THF (10 ml) and a solution of **1** (3.09 g, 10.2 mmol) in THF (20 ml). The solution was allowed to warm to room temperature, stirred overnight, and concentrated under reduced pressure. The residue was triturated several times with DCM (10 ml), and further purification by chromatography on silica gel (DCM/MeOH, 97:3) afforded the product as a white solid (2.70 g, 70%). ^{1}H NMR (400 MHz, CD_3OD) δ 7.25 to 7.50 (15H, m), 3.76 (2H, t, J = 5.4 Hz), 2.72 (2H, t, J = 5.5 Hz), 1.29 (3H, d, J = 16.8 Hz); ^{13}C NMR (100 MHz, CD_3OD) δ 142.5, 129.4, 128.9, 128.5, 73.9, 58.9, 47.8, 12.6 (d, J = 139 Hz).

2-Aminoethyl methylphosphonate (3). Compound **2** (1.00 g, 2.62 mmol) was dissolved in 20 ml of trifluoroacetic acid in DCM [5% (v/v)]. The solution was stirred for 20 min and then concentrated. Hexane (30 ml) was added, the mixture was vigorously stirred at 50°C, and then the hexane layer was removed. This process was repeated several times, and traces of hexane were removed under reduced pressure to afford the product as a clear oil (0.35 g, 97%). Spectral data matched those reported previously (Chowdhury et al., 2007).

(*S*)-1-(Benzyloxycarboxamido)propan-2-ol [(*S*)-4]. To a solution of (*S*)-1-aminopropan-2-ol (1.41 g, 18.8 mmol) in anhydrous THF (30 ml) was added benzyl chloroformate (3.9 ml, 28.2 mmol) and DIPEA (4.9 ml, 28.2 mmol) at 0°C. The solution was allowed to warm slowly to room temperature and stirred overnight. After dilution with EtOAc (50 ml), the reaction mixture was washed with deionized water (2 × 30 ml) and brine (20 ml), then dried over Na_2SO_4 and concentrated to give a clear oil. Purification by chromatography (DCM/MeOH, 98:2) afforded the product as a clear oil (3.12 g, 80%). ^{1}H NMR (400 MHz, $CDCl_3$) δ 7.30 to 7.40 (5H, m), 5.63 (1H, br s), 5.08 (2H, s), 3.86 (1H, br s), 3.41 (1H, br s), 3.25 to 3.38 (1H, m), 3.00 to 3.13 (1H, m), 1.14 (3H, d, J = 6.2 Hz); ^{13}C NMR (100 MHz, $CDCl_3$) δ 158.2, 137.3, 129.3, 128.9, 128.8, 67.4, 67.2, 48.5, 20.6.

(*R*)-1-(Benzyloxycarboxamido)propan-2-ol [(*R*)-4]. By the same procedure employed for (*S*)-**4,** 1.84 g (83%) of (*R*)-**4** was obtained from 0.80 g (10.6 mmol) of (*R*)-1-aminopropan-2-ol. ^{1}H and ^{13}C NMR spectra were identical with those of the enantiomeric (*S*)-**4**.

(*R*)-2-(Benzyloxycarboxamido)-1-methylethyl methylphosphonate [(R)-5]. To a solution of triphenylphosphine (0.621 g, 2.37 mmol), methylphosphonic acid (0.151 g, 1.58 mmol) and alcohol (*S*)-**4** (0.330 g, 1.58 mmol) in THF (15 ml) was added DEAD (1.08 ml, 40% solution in toluene, 12.2 mmol) at 0°C. The solution was allowed to warm slowly to room temperature and stirred for 4 h. After dilution with EtOAc (30 ml), the reaction mixture was washed with deionized water (2 × 30 ml) and brine (20 ml), then dried over Na_2SO_4 and concentrated to give a light-yellow oil. Purification by chromatography (DCM/MeOH, 90:10) afforded the product as a clear oil (0.340 g, 75%). ^{1}H NMR (400 MHz, CD_3OD) δ 7.20 to 7.55 (5H, m), 5.07 (2H, s), 4.40 to 4.55 (1H, m), 3.90 to 4.07 (1H, m), 3.13 to 3.33 (1H, m), 1.41 (3H, d, J = 17.2 Hz), 1.29 (3H, d, J = 6.3 Hz); ^{13}C NMR (100 MHz, CD_3OD) δ 158.5, 137.7, 128.8, 128.4, 128.3, 72.3, 66.5, 46.6, 18.5, 10.8 (d, J = 144.1 Hz).

(*S*)-2-(Benzyloxycarboxamido)-1-methylethyl methylphosphonate [(*S*)-5]. By the same procedure used for (*R*)-**5**, 0.243 g (81%) of (*S*)-**5** was obtained from 0.218 g (1.04 mmol) of (*R*)-**4**. ^{1}H and ^{13}C NMR spectra were identical with those of the enantiomeric (*R*)-**5**.

(*R*)-2-Amino-1-methylethyl methylphosphonate [(*R*)-6]. A flask charged with (*R*)-**5** (0.119 g, 0.41 mmol) and 10% Pd-C (6 mg) was flushed with hydrogen for 15 min, after which methanol (10 ml) was introduced. The mixture was stirred vigorously under a hydrogen atmosphere for 2 h, the solid was removed by filtration, and the solution was concentrated under reduced pressure to afford the product as a clear oil (0.059 g, 94%). ^{1}H NMR (400 MHz, CD_3OD) δ 4.40 to 4.60 (1H, m), 3.04 (1H, dd, J = 13.1, 2.4 Hz), 2.87 (1H, dd, J = 13.1, 8.9 Hz), 1.294 (3H, d, J = 6.4 Hz) 1.286 (3H, d, J = 16.6 Hz); ^{13}C NMR (100 MHz, CD_3OD) δ 67.7, 45.6, 18.7, 12.1 (d, J = 139.9 Hz).

(*S*)-2-Amino-1-methylethyl methylphosphonate [(*S*)-6]. By the same procedure employed for (*R*)-**6**, 0.100 g (96%) of (*S*)-**6** was obtained from 0.200 g (0.690 mmol) of (*S*)-**5**. ^{1}H and ^{13}C NMR spectra were identical with those of the enantiomeric (*R*)-**6**.

Methyl methylphosphonate (7). Demethylation of dimethyl methylphosphonate was performed using a modification of the procedure described by Krawczyk (1997). To a solution of dimethyl methylphosphonate (5.00 g, 40.0 mmol) in acetone (200 ml) was added lithium bromide (5.25 g, 60.0 mmol). The mixture was refluxed overnight, cooled, and filtered to collect the lithium salt of the product, which was dissolved in methanol and stirred with Dowex 50WX8 ion exchange resin (acid form, prewashed with ethanol) for 30 min. Filtration and evaporation of the solvent afforded the product as a light yellow oil. Further purification by chromatography (DCM/MeOH, 90:10) afforded a clear oil (4.31 g, 97%). ^{1}H NMR (400 MHz, $CDCl_3$) δ 3.68 (3H, d, J = 10.7 Hz), 1.45 (3H, d, J = 17.8 Hz); ^{13}C NMR (100 MHz, $CDCl_3$) δ 51.1, 9.4 (d, J = 143.5 Hz).

(*R*)-2-(Benzyloxycarboxamido)propan-1-ol [(*R*)-8]. To a stirred solution of (*R*)-2-aminopropan-1-ol (1.00 g, 13.3 mmol) in anhydrous THF (20 ml) was added benzyl chloroformate (2.80 ml, 19.9 mmol) and DIPEA (3.48 ml, 19.9 mmol) at 0°C. The solution was allowed to warm slowly to room temperature and then stirred overnight. After dilution with EtOAc (40 ml), the reaction mixture was washed with deionized water (2 × 20 ml) and brine (10 ml), then dried over Na_2SO_4 and concentrated to give a clear oil. Purification by chromatography (DCM/MeOH, 98:2) afforded the product as a clear oil (2.42 g, 87%). ^{1}H NMR (400 MHz, CD_3OD) δ 7.15 to 7.40 (5H, m), 5.07 (2H, s), 3.65 to 3.8 (1H, m), 3.40 to 3.55 (2H, m), 1.13 (3H, d, J = 6.8 Hz); ^{13}C NMR (100 MHz, CD_3OD) δ 158.0, 137.8, 128.9, 128.4, 128.2, 66.4, 65.4, 48.9, 16.3.

(*S*)-2-(Benzyloxycarboxamido)propan-1-ol [(*S*)-8]. By the same procedure used for (*R*)-**8**, 2.54 g (91%) of (*S*)-**8** was obtained from 1.00 g (13.3 mmol) of (*S*)-2-aminopropan-1-ol. ^{1}H and ^{13}C NMR spectra were identical with those of the enantiomeric (*R*)-**8**.

(2*R*)-2-(Benzyloxycarboxamido)propyl methyl methylphosphonate [(2*R*)-9]. To a solution of **7** (0.393 g, 3.57 mmol) in THF (10 ml) at room temperature under a nitrogen atmosphere were added (*R*)-**8** (0.747 g, 3.57 mmol) and triphenylphosphine (1.12 g, 4.28 mmol). DEAD (0.745 g, 4.28 mmol) was added drop-wise, and the solution was stirred overnight. After dilution with EtOAc (40 ml), the reaction mixture was washed with deionized water (2 × 20 ml) and brine (15 ml) and then dried over Na_2SO_4 and concentrated to give a yellow oil. Purification by chromatography (EtOAc) afforded the product as a colorless solid (0.89 g, 83%). The product is an approximately 60:40 mixture of configurations at phosphorus; NMR resonances are not distinguishable except where indicated. ^{1}H NMR (400 MHz, CD_3OD) δ 7.25 to 7.45 (5H, m), 5.00 to 5.15 (2H, m), 3.85 to 4.05 (3H, m), 3.70 (3H, d, J = 11.1 Hz, minor isomer), 3.69 (3H, d, J = 11.1 Hz; major isomer), 1.50 (3H, d, J = 17.6 Hz, minor isomer), 1.48 (3H, d, J = 17.6 Hz, major isomer), 1.19 (3H, d, J = 6.6 Hz); ^{13}C NMR (100 MHz, CD_3OD) δ 157.8, 128.8, 128.4, 128.3, 68.4, 66.4, 51.9, 47.1 15.6, 8.26 (d, J = 144.9 Hz, minor isomer), 8.21 (d, J = 145.0 Hz, major isomer).

(2*S*)-2-(Benzyloxycarboxamido)propyl methyl methylphosphonate [(2*S*)-9]. By the same procedure used for (2*R*)-**9**, 2.10 g (89%) of (2*S*)-**9** was obtained from 1.63 g (7.79 mmol) of (*S*)-**8**. ^{1}H and ^{13}C NMR spectra were identical with those of the enantiomeric (2*R*)-**9**.

(*R*)-2-(Benzyloxycarboxamido)propyl methylphosphonate [(*R*)-10]. To a solution of (2*R*)-**9** (1.15 g, 3.8 mmol) in anhydrous THF (10 ml) under a nitrogen atmosphere was added drop-wise LiHB(*s*-Bu)$_3$ (1.0 M in THF, 8.76 ml, 8.76 mmol), and the solution was stirred

for 4 h. After removal of the solvent under reduced pressure, the residue was dissolved in methanol (20 ml) and stirred with Dowex 50WX8 ion exchange resin (acid form, prewashed with ethanol) for 30 min. Filtration followed by evaporation of the solvent and purification by chromatography on silica gel (DCM/MeOH, 99:1) afforded the product as a clear oil (0.81g, 74%). ^{1}H NMR (400 MHz, CD_3OD) δ 7.25 to 7.40 (5H, m), 5.06 (2H, s), 3.80 to 3.90 (3H, m), 1.42 (3H, d, J = 17.5 Hz), 1.17 (3H, d, J = 6.4 Hz); ^{13}C NMR (100 MHz, CD_3OD) δ 157.8, 137.7, 128.8, 128.3, 128.2, 67.6, 66.4, 15.8, 9.9 (d, J = 143.6 Hz).

(*S*)-2-(Benzyloxycarboxamido)propyl methylphosphonate [(*S*)-10]. By the same procedure used for (*R*)-**10**, 1.58 g (83%) of (*S*)-**10** was obtained from 2.00 g (6.60 mmol) of (*S*)-**9**. ^{1}H and ^{13}C NMR spectra were identical with those of the enantiomeric (*R*)-**10**.

(*R*)-2-Aminopropyl methylphosphonate [(*R*)-11]. A flask charged with (*R*)-**10** (0.530 g, 1.85 mmol) and 10% Pd/C (0.027 g, 5 weight percent) was flushed with hydrogen for 15 min, after which methanol (20 ml) was introduced. The mixture was stirred vigorously under a hydrogen atmosphere for 2 h, the solid was removed by filtration, and the solution was concentrated under reduced pressure to afford the product as a clear oil (0.275 g, 97%). ^{1}H NMR (400 MHz, CD_3OD) δ 3.97 to 4.03 (1H, m), 3.74 to 3.82 (1H, m), 3.43 to 3.51 (1H, m), 1.290 (3H, d, J = 6.8 Hz) 1.285 (3H, d, J = 16.6 Hz); ^{13}C NMR (100 MHz, CD_3OD) δ 64.9, 48.3, 13.9, 11.0 (d, J = 139.1 Hz).

(*S*)-2-Aminopropyl methylphosphonate [(*S*)-11]. By the same procedure used for (*R*)-**11**, 0.235 g (99%) of (*S*)-**11** was obtained from 0.444 g (1.55 mmol) of (*S*)-**10**. ^{1}H and ^{13}C NMR spectra were identical with those of the enantiomeric (*R*)-**11**.

2-Aminoethyl benzylphosphonate (12). To a solution of benzylphosphonic acid (0.1997 g, 1.16 mmol) in *N*,*N*-dimethylformamide (2 ml) was added a solution of aziridine (50 mg, 1.16 mmol) in *N*,*N*-dimethylformamide (0.5 ml), and the solution was stirred at room temperature overnight. The product precipitated as white solid that was collected and washed with acetone (0.141 g, 55%). Spectral data matched those reported previously (Chowdhury et al., 2007).

2-(Triphenylmethylamino)ethyl *n*-butylphosphonic acid (13). To a solution of *n*-butylphosphonic acid (1.62 g, 11.7 mmol) and 2-(triphenylmethylamino)ethanol (3.55 g, 11.7 mmol) in anhydrous THF (50 ml) at 0°C was added triphenylphosphine (3.63 g, 14.0 mmol) and, drop-wise, DEAD (2.45 g, 13.8 mmol). The solution was allowed to warm to room temperature, stirred overnight, diluted with ethyl acetate, washed twice with water and once with brine, then concentrated under reduced pressure. The residue was purified by chromatography on silica gel (DCM/MeOH, 98:2) to afford 4.3 g (87%) of the product. ^{1}H NMR (400 MHz, $CDCl_3$) δ 7.46 (6H, dt, J = 7.2, 1.6 Hz), 7.26 (6H, tt, J = 7.4, 1.5 Hz), 7.17 (3H, tt, J = 7.4, 1.5 Hz), 3.97 (2H, q, J = 5.6 Hz), 2.35 (2H, t, J = 5.4 Hz), 1.48 to 1.62 (4H, m), 1.38 (2H, sx, J = 7.0 Hz), 0.91 (3H, t, J = 7.4 Hz); ^{13}C NMR (100 MHz, $CDCl_3$) δ: 145.6. 128.5, 127.6, 126.2, 70.6, 64.2, 44.2, 26.5 (d, J = 135 Hz), 26.0 (d, J = 5.3 Hz), 24.1 (d, J = 17.2 Hz), 13.8.

2-Aminoethyl n-butylphosphonic acid (14). To a solution of 2-(triphenylmethylamino)ethyl *n*-butylphosphonic acid (**13**, 142 mg, 0.34 mmol) in DCM (15 ml) was added trifluoroacetic acid (1 ml) drop-wise. The solution was stirred for 30 min at room temperature and then concentrated under reduced pressure to a yellow oil, which was redissolved in methanol (5 ml), concentrated under reduced pressure, and left in vacuo for 30 min. The solidified residue was extracted five times with 7-ml portions of hexanes at 50°C, leaving a colorless, slightly cloudy oil. Removal of residual solvent in vacuo afforded a trifluoroacetate salt of the product as a colorless oil in essentially quantitative yield. ^{1}H NMR (400 MHz, CD_3OD) δ: 4.14 to 4.20 (2H, m), 3.20 (2H, br t, J = 5.0 Hz), 1.68 to 1.79 (2H, m), 1.52 to 1.64 (2H, m), 1.37 to 1.48 (2H, m), 0.93 (3H, t, J = 7.2 Hz); ^{13}C NMR (100 MHz, CD_3OD) δ: 162.3 (q, J = 35.8 Hz, F_3CCO_2H), 118.0 (q, J = 292 Hz, F_3CCO_2H), 61.9 (d, J = 6.2 Hz), 41.5 (d, J = 6.1 Hz), 26.8 (d, J = 138 Hz), 26.0 (d, J = 6.2 Hz), 24.9 (d, J = 18.3 Hz), 14.0.

Electrophysiology. Membrane currents of neuroblastoma cells were obtained by whole-cell voltage-clamp recording at a holding potential of −60 mV. Cells were superfused (~1 ml/min) with physiological saline (mammalian Ringer solution) that consisted of 135 mM NaCl, 5 mM KCl, 2 mM $CaCl_2$, 2 mM $MgCl_2$, 5 mM HEPES, and 10 mM glucose, pH 7.4. In all experiments, the recorded cell was adherent to the floor of the recording chamber. The patch pipette was filled with an intracellular solution containing 140 mM CsCl, 4 mM KCl, 1 mM $CaCl_2$, 2 mM $MgCl_2$, 11 mM EGTA, and 10 mM HEPES, pH 7.2. The pipette resistance was 7 to 8 MΩ. Data were acquired with an Axopatch 200B amplifier controlled by pCLAMP software (Molecular Devices, Sunnyvale, CA). Recordings were filtered at 1 kHz, and the digitization frequency was 2.5 kHz. The data were analyzed and plotted using OriginPro 7.5 software (OriginLab Corp, Northampton, MA). Test agents dissolved in Ringer solution were delivered to the cell by a computer-controlled perfusion system (SF-77B; Warner Instruments, Hamden, CT). To determine the kinetics of the delivery system, we measured the change in junction potential measured by an electrode held at a fixed position in the recording chamber when the perfusing medium was switched from mammalian Ringer solution to a solution containing 100 mM isethionic acid; measurements obtained with three different electrodes yielded 39 ± 15 ms (n = 3) as the exponential time constant of junction potential change. We also determined the solution exchange time exhibited by $GABA_A$-ρ1-expressing neuroblastoma cells. For each of four cells, we analyzed the membrane-current response induced by a switch from mammalian Ringer into a Ringer solution supplemented with 100 mM potassium gluconate. These cell measurements yielded an exponential time constant of 102 ± 28 ms.

In addition to the synthesized test compounds (see above), the experiments used GABA (Sigma-Aldrich, St. Louis, MO), muscimol (Tocris Bioscience, Ellisville, MO), TPMPA (Sigma-Aldrich), and 3-APMPA (Tocris Bioscience). The inhibitory effect of a given test agent on the GABA-elicited response was examined by varying the concentration of test agent coapplied with a fixed concentration of GABA; normalized peak amplitudes of the resulting responses were analyzed through a Hill-type equation,

$$r/r_{max} = [IC_{50}]^h/\{[c]^h + [IC_{50}]^h\} \quad (1)$$

where r/r_{max} is the normalized peak amplitude, [c] is the concentration of test agent, and the parameter $[IC_{50}]$ and the Hill coefficient h are fitted parameters. The GABA response function in the presence of a fixed concentration of test agent was determined by analyzing normalized peak amplitudes of the response through a similar equation,

$$r/r_{max} = [GABA]^h/\{[GABA]^h + [EC_{50}]^h\} \quad (2)$$

where the parameter $[EC_{50}]$ and Hill coefficient h are fitted parameters. Procedures for the preparation of $GABA_A$-ρ1- and $\alpha1\beta2\gamma2$ $GABA_A$-expressing *X. laevis* oocytes and for two-electrode voltage-clamp recording from the oocytes were similar to those described previously (Vu et al., 2005; Chowdhury et al., 2007).

Competition Binding. $GABA_A$-ρ1-expressing neuroblastoma cells and control, nonexpressing cells were analyzed for the displacement of [^{3}H]muscimol or [^{3}H]GABA by 2-AEMP in competition binding experiments. [^{3}H]GABA was obtained from GE Healthcare (Chalfont St. Giles, Buckinghamshire, UK), and [^{3}H]muscimol was from PerkinElmer Life and Analytical Sciences (Waltham, MA); unlabeled GABA and muscimol were products of Sigma-Aldrich. Procedures used were similar to those described previously (Khasawneh et al., 2006, 2008), with minor modifications to optimize [^{3}H]muscimol and [^{3}H]GABA binding in the present system. In brief, the cells were seeded on poly(L-lysine)-coated 12-well plates. Upon reaching confluence, the cells were washed twice with ice-cold buffer containing 50 mM Tris-HCl and 5 mM $MgCl_2$, pH 7.4. Cells were preincubated with various concentrations of 2-AEMP (0.5–500 μM) for 5 min on ice followed by incubation with either [^{3}H]muscimol (20 nM) or [^{3}H]GABA (40 nM) for 1 h at 4°C with gentle shaking. The cells were then rapidly washed two times (with the above buffer), and 500 μl of 0.3 N

NaOH plus 0.1% EDTA was added. The plates were shaken for 10 min at 4°C to detach the cells, and 100 μl of 10 N HCl was added to neutralize the pH. The solubilized cell solution was then transferred to vials containing 8 ml of scintillation fluid and analyzed for radioactivity in a Beckman LS 6500 liquid scintillation counter (Beckman Coulter, Fullerton, CA). Nonspecific binding was determined using a 1000-fold molar excess of unlabeled GABA or muscimol (2 μM) and was typically 40% of the total binding.

Modeling of Ligand Docking. Docking of the ligands at the human GABA$_A$-ρ1 receptor was performed using the Glide 5.0 package (Schrödinger LLC, New York, NY) as described previously (Halgren et al., 2004; Friesner et al., 2004; Abdel-Halim et al., 2008). The antagonist-minimized model of GABA$_A$-ρ1 (Abdel-Halim et al., 2008) was imported into the Maestro 8.5 graphical user interface (Schrödinger LLC). A grid representing the shape and properties of the binding site was generated using the grid generation module in Glide. The grid to be used for docking was determined as the centroid of the major binding residues: Tyr102, Arg104, Trp133, Pro135, Asp136, Phe138, Phe139, Val140, Ser142, Phe146, Ser168, Arg170, Tyr198, Tyr200, Tyr241, Ser243, Thr244, and Tyr247 (Amin and Weiss, 1994, 1996; Torres and Weiss, 2002; Sedelnikova et al., 2005; Harrison and Lummis, 2006). The Coulomb-van der Waals radii of the receptor residues were set to 1.0.

Each ligand was docked on the generated grid. Ligands were built using the Maestro 8.5 graphical user interface (Schrödinger LLC) and were energy-minimized with the MacroModel 9.6 module (MacroModel, version 9.6; Schrödinger LLC) using the OPLS 2005 force field (Jorgensen et al., 1996). Docking was then performed using the extra-precision function (Friesner et al., 2006) and a multiplier of 1.0 for van der Waals radii of the ligands. In all but one case, ligands were successfully docked with this approach; in the case of benzyl analog **12**, a reduction of the van der Waals multiplier to 0.7 was required for successful docking. The docking process typically produced four to six poses of similar energy. Output sets were manually filtered to select only those maintaining hydrogen bonds to Arg104 and Tyr198, which have been observed for all active compounds docked with the antagonist model (Abdel-Halim et al., 2008). One representative pose for each compound was selected for illustration under *Results*.

Results

Chemical Synthesis. In this study we sought to compare the parent 2-AEMP (**3**) with derivatives substituted at each of its three carbon atoms. The two carbon atoms of the aminoethyl side chain bear four chemically distinct hydrogen atoms, each of which was substituted with a methyl group [compounds (*R*)-**6**, (*S*)-**6**, (*R*)-**11**, and (*S*)-**11**]. The methyl substituent at phosphorus was replaced with longer linear (*n*-butyl) and branched (benzyl) groups (compounds **14** and **12**, respectively). Four different synthetic approaches were used for the aminoethyl phosphonates. 2-AEMP (**3**) was prepared by an improved method (Fig. 2A), in which the key step was coupling of methylphosphonic acid and *N*-trityl-2-aminoethanol via the Mitsunobu reaction. Removal of the trityl group afforded the product in 68% yield for the two steps. *n*-Butylphosphonate (**14**) was made in an analogous manner. Compounds (*R*)-**6** and (*S*)-**6** were prepared by a mono-Mitsunobu coupling of methylphosphonic acid with the appropriate enantiomer of *N*-Cbz-protected 1-amino-2-propanol [(*S*)-**4** or (*R*)-**4**, respectively], with presumed inversion at carbon-2 (Fig. 2B). Hydrogenolytic removal of the protecting group afforded the products in 78% [(*R*)-**6**] or 70% [(*S*)-**6**] yield for the two steps. Compounds (*R*)-**11** and (*S*)-**11** were prepared by Mitsunobu coupling between methyl methylphosphonate and the appropriate enantiomer of *N*-Cbz-protected 2-amino-1-propanol (Fig. 2C). O-Demethylation using Li(*s*-Bu)$_3$BH, as described in Chowdhury et al. (2007), followed by hydrogenolytic removal of the Cbz group, afforded the products in 73% [(*R*)-**11**] or 60% [(*S*)-**11**] yield over the three steps. Finally, 2-aminoethyl benzylphosphonate (**12**) was synthesized in 55% yield in a single step by reaction of benzylphosphonic acid with aziridine using an adaptation of the procedure described by Cates et al. (1984) for preparation of 2-aminoethyl phenylphosphonate (Fig. 2D). This simple procedure

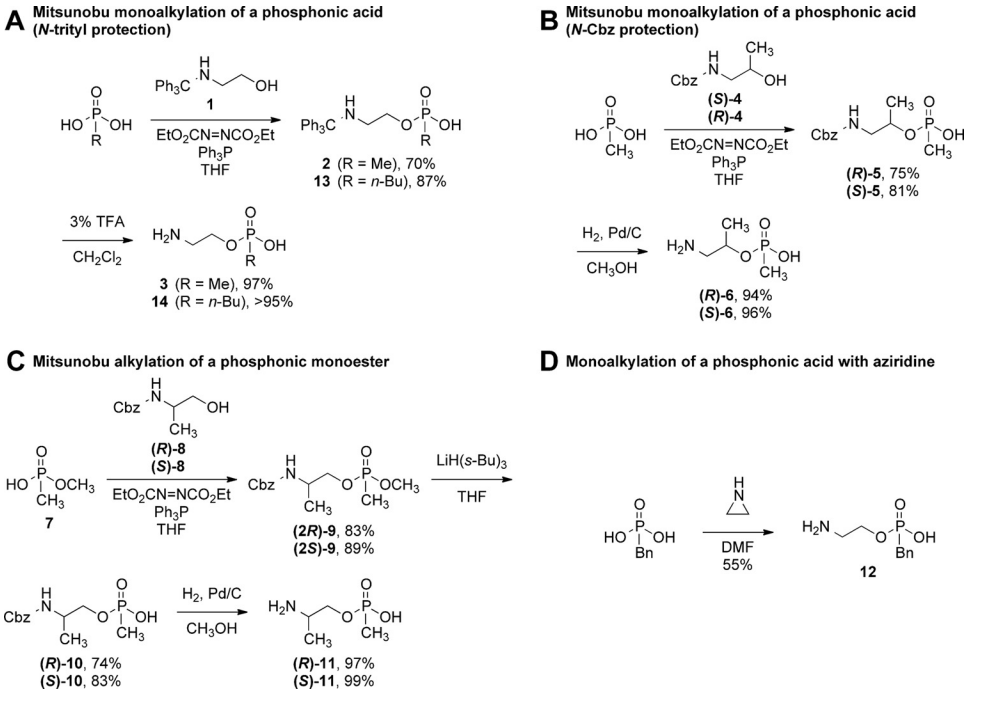

Fig. 2. Synthesis of 2-aminoethyl methylphosphonate (2-AEMP, **3**) and investigated analogs. Four variants (A–D) of the synthetic approach were used; captions indicate the key bond-forming step in each.

failed with methylphosphonic acid, so 2-AEMP could not be synthesized in the same manner.

Electrophysiology and Competition Binding. Electrophysiological experiments were undertaken to characterize the actions of 2-AEMP and analogs at the $GABA_A$-ρ1 receptor. These experiments began with the determination of inhibition constants, and then progressed to the kinetics of interaction between 2-AEMP and $GABA_A$-ρ1, with the latter revealing significant differences in the pharmacology of 2-AEMP and TPMPA.

We determined inhibition constants at two different GABA concentrations, 1 and 10 μM. Figure 3A illustrates the effect of 2-AEMP on GABA-elicited currents. The waveforms shown in the upper portion of Fig. 3A were recorded from a single cell in response to, sequentially, 10 μM GABA (trace 1), 10 μM GABA plus 100 μM 2-AEMP (trace 2), and 10 μM GABA (trace 3). As illustrated by these data, coapplication of the 2-AEMP with 10 μM GABA produced a pronounced inhibition of the GABA-elicited response, and this inhibition was fully reversible. Waveforms shown in the lower portion of Fig. 3A illustrate the inhibition, by 2-AEMP, of the response to a fixed 1-μM concentration of GABA. By analyzing peak currents of waveforms obtained with a range of 2-AEMP concentrations, we determined the inhibition functions shown in Fig. 3B. As further described below, the rate of block of the GABA response by coapplied antagonist (in Fig. 3B, 2-AEMP), as well as rates of desensitization and deactivation kinetics of the GABA response, differed noticeably among the investigated cells. However, neither the analysis yielding the Fig. 3B inhibition functions nor those yielding other aggregate data presented below involved selection of cells exhibiting, for example, relatively fast or relatively slow rates of the investigated parameter. In Fig. 3B, analysis of the normalized, aggregate data through eq. 1 yielded an IC_{50} value of 18.1 $\pm$ 4.5 μM and a Hill coefficient of 0.78 $\pm$ 0.14 (n = 5) for 2-AEMP coapplied with 10 μM GABA and an IC_{50} of 0.40 $\pm$ 0.11 μM and a Hill coefficient of 0.74 $\pm$ 0.13 for 2-AEMP coapplied with1 μM GABA. The responses leading to the determination of the dose-response curves in Fig. 3B, and in the experiments described below, often did not reach a full peak (e.g., response 2 in the top and bottom parts of Fig. 3A) during the several-second period of application of the test agent(s). This absence of full peak development was a consequence of the periods of treatment with coapplied GABA plus antagonist in a given experimental run, a design used to preserve cell viability over a full series of test treatments. In the experiment of Fig. 3 and below, the measurement of peak amplitude in the absence of full peak development can be expected to introduce some bias in the reported values of IC_{50}, EC_{50}, and Hill coefficient.

The action of 2-AEMP was further examined in radioligand binding experiments using [^{3}H]GABA as a probe (Fig. 3C). Here, a fixed amount of [^{3}H]GABA was accompanied by increasing concentrations of 2-AEMP in a competition binding assay. To calculate the specific binding (which was approximately 60%), the same concentration of radioligand was competed against a 1000-fold molar excess of unlabeled muscimol or GABA. Increasing the 2-AEMP concentration progressively reduced the binding of [^{3}H]GABA ligand (●). The data were analyzed through the equation (see eqs. 1 and 2)

$$B/B_{\max} = [IC_{50}]^h/\{[2\text{-AEMP}]^h + [IC_{50}]^h\} \quad (3)$$

where B is the absolute value of specific binding, $B_{\max}$ is the maximal level of binding, and IC_{50}, h, and $B_{\max}$ are free parameters. This fitting yielded IC_{50} = 19.8 $\pm$ 0.4 μM and h = 0.8 $\pm$ 0.1 (n = 2). 2-AEMP also competed with [^{3}H]muscimol binding in dose-dependent manner (▲) and yielded IC_{50} = 17.8 $\pm$ 0.7 μM and h = 0.9 $\pm$ 0.1.

We next compared the inhibitory action of 2-AEMP with those of phosphinic $GABA_A$-ρ1 antagonists 3-APMPA and TPMPA described previously (Ragozzino et al., 1996). The representative waveforms shown in Fig. 4A illustrate the inhibitory effect of 10 μM TPMPA, 10 μM 3-APMPA, and 10 μM 2-AEMP on the response of a single cell to 10 μM GABA. Figure 4B shows inhibition functions for peak amplitude determined from experiments that used a fixed, 10-μM concentration of GABA and varying concentrations of TPMPA (△) or 3-APMPA (○). For reference, the 2-AEMP data of Fig. 3B are also included here. Analysis of the Fig. 4B data

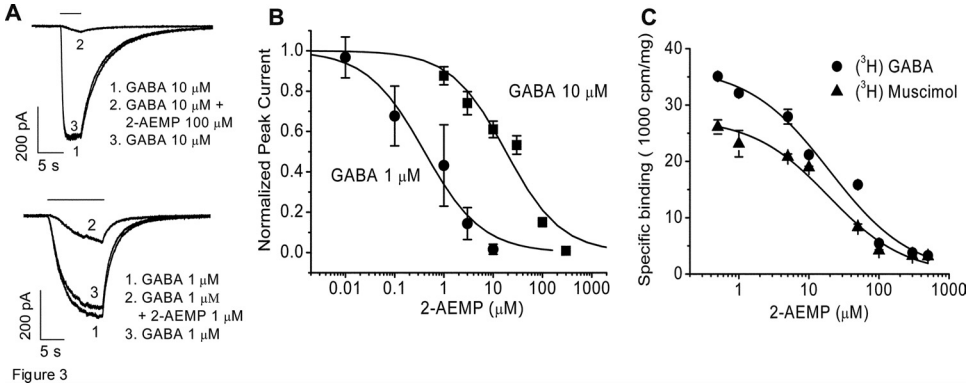

Figure 3

Fig. 3. Inhibitory effect of 2-AEMP on GABA-elicited responses. A, top, responses recorded from a single cell upon treatment with 10 μM GABA alone or coapplied 10 μM GABA plus 100 μM 2-AEMP. Response 1 was obtained before, and response 3 after, the response to the GABA plus 2-AEMP mixture (response 2). Bottom, responses recorded from a second cell upon treatment, sequentially, with 1 μM GABA alone (trace 1), 1 μM GABA plus 1 μM 2-AEMP (trace 2), and 1 μM GABA (trace 3). B, inhibition functions for 2-AEMP obtained with 10 μM GABA (■; means $\pm$ S.D. for peak amplitudes of currents obtained from five cells, including that described in the top of A) and with 1 μM GABA (●; data obtained from five cells, including that described at the bottom of A). Curves illustrate the fit of eq. 1 to the data. C, competition binding data obtained with varying concentration of 2-AEMP in the presence of 40 nM [^{3}H]GABA (●) or of 20 nM [^{3}H]muscimol (▲). Each set of data shows means $\pm$ S.D. determined in two experiments. The illustrated curve shown for each radioligand represents eq. 3 fitted to the data; analysis through the fitting software (Origin 7.5) provided the results quoted in the accompanying text.

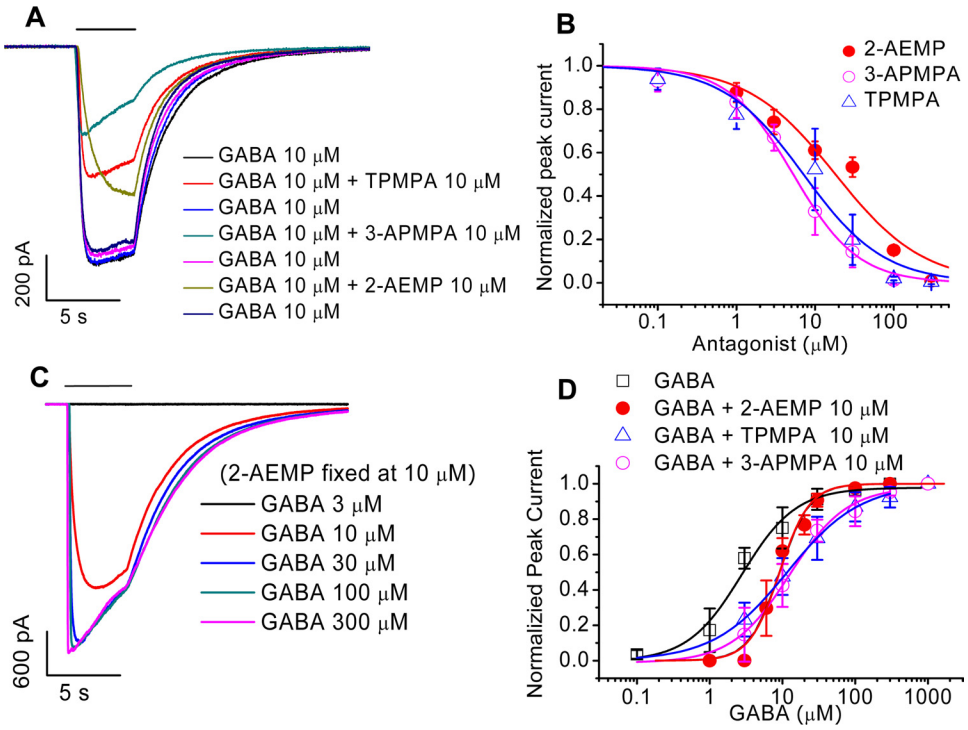

Fig. 4. Comparative action of 2-AEMP, 3-APMPA, and TPMPA on GABA-elicited responses. A, effects of 10 μM TPMPA, 3-APMPA, and 2-AEMP on the response elicited by 10 μM GABA. Data obtained from a single cell on presentation of the test agents described in the key. Top-to-bottom order of the labels shown in the key indicates the sequence of the treatments. B, inhibition functions for TPMPA (△) and 3-APMPA (○) obtained with 10 μM GABA. Curves illustrate the fit of eq. 1 to the data. Here and in D, the illustrated data represent determinations of peak response amplitude. For comparison, the function for 2-AEMP (red filled circles) is replicated from Fig. 3B. C, effect of 2-AEMP at fixed concentration (10 μM) on responses to varying concentrations of GABA. Data obtained from a single cell. D, GABA response functions obtained with GABA alone (□, $n = 5$) or with co-application of a fixed 10 μM concentration of 2-AEMP (red filled circles, $n = 3$), TPMPA (△, $n = 5$), or 3-APMPA (○, $n = 5$). Curves illustrate the fit of eq. 2 to the data.

through eq. 1 yielded an IC_{50} of 7.1 ± 1.7 μM with a Hill coefficient of 1.22 ± 0.20 ($n = 5$) for TPMPA and an IC_{50} of 5.3 ± 0.4 μM with a Hill coefficient of 1.05 ± 0.09 ($n = 6$) for 3-APMPA. These results may be compared with those of a previous study that tested the potency of 2-AEMP and TPMPA at GABA$_A$-ρ1 receptors expressed in *X. laevis* oocytes (Chowdhury et al., 2007). That earlier study yielded IC_{50} values of 11.1 μM for 2-AEMP and 0.67 μM for TPMPA when tested in the presence of 1 μM GABA. The differences in relative potencies of the two compounds in *X. laevis* oocytes (Chowdhury et al., 2007) and in neuroblastoma cells (Fig. 4) could reflect differing microenvironments of the GABA$_A$-ρ1 receptor in the two expression systems.

Further comparison was made by evaluating the GABA response function in which the GABA concentration, rather than the inhibitor concentration, was varied. Figure 4, C and D, shows representative waveforms (C) and the GABA response function for peak amplitude (D) obtained with a fixed, 10-μM concentration of 2-AEMP. The normalized GABA response function obtained with 2-AEMP using eq. 2 exhibited a rightward shift (EC_{50} = 8.6 ± 0.8 μM) and a substantial increase in Hill coefficient (2.3 ± 0.4; $n = 3$) by comparison with the function obtained in the absence of antagonist [EC_{50} of 2.8 ± 0.5 μM; Hill coefficient of 1.2 ± 0.2 ($n = 5$)]. By contrast, normalized response functions obtained with TPMPA (△) and 3-APMPA (○) exhibited approximately equal rightward shifts relative to the GABA response function and little change in Hill coefficient [for 3-APMPA, EC_{50} of 12.7 ± 1.5 μM, and Hill coefficient of 1.2 ± 0.2 ($n = 5$); for TPMPA, EC_{50} of 11.5 ± 2.0 μM and Hill coefficient of 1.0 ± 0.2 ($n = 5$)]. It should be noted that some of the responses leading to the Fig. 4, C and D, response functions did not develop a full peak during the period of treatment with GABA alone or with coapplied antagonist, and this absence of a full peak may introduce some quantitative bias into determination of the response functions describing peak amplitudes. However, the increase in Hill coefficient determined with 2-AEMP (Fig. 4) suggests a subtle but significant difference between 2-AEMP's mode of interaction with the receptor and that of the phosphinic antagonists. In addition, there was an indication of a small, possibly noncompetitive component of 2-AEMP's antagonist activity. That is, at high GABA concentration (300 μM), the peak current obtained with coapplied 100 μM 2-AEMP represented 86 ± 9% of that obtained with GABA alone.

In experiments similar to those of Fig. 4D, we tested the effect of 2-AEMP at fixed concentration (100 μM) on GABA responses of GABA$_A$-ρ1 receptors expressed in *X. laevis* oocytes, and analyzed the normalized peak currents determined in these experiments through eq. 2. In the absence of 2-AEMP, the normalized GABA response function exhibited an EC_{50} of 1.2 ± 0.0 μM and a Hill coefficient of 1.6 ± 0.1 ($n = 4$), whereas the function obtained with coapplied 100 μM 2-AEMP yielded an EC_{50} of 4.7 ± 0.2 μM and a Hill coefficient of 2.5 ± 0.1 ($n = 4$). The effects on EC_{50} and Hill coefficient produced by 100 μM 2-AEMP in the GABA$_A$-ρ1-expressing oocytes were thus generally similar to that produced by 10 μM 2-AEMP in the GABA$_A$-ρ1-expressing neuroblastoma cells. We also tested the effect of 2-AEMP on oocytes expressing $\alpha1\beta2\gamma2$ GABA$_A$ receptors. Consistent with information reported previously (Chowdhury et al., 2007), 100 μM 2-AEMP had no significant effect on the response elicited by 10 μM GABA (data not shown).

We next undertook a set of experiments to examine further properties of the inhibition produced by 2-AEMP. Another approach to determining whether antagonism by an inhibitory test agent is primarily competitive versus noncompetitive is to examine the effect of introducing the test agent during washout of the nominal ligand (here, GABA). That is, if 2-AEMP rapidly binds and deactivates the GABA-activated state of the receptor, its addition during the washout phase would accelerate deactivation. On the other hand, if 2-AEMP

competes with GABA, its addition during the washout phase would not alter the rate of deactivation. Figure 5 shows representative results obtained in an experiment of the type just described. Here, 2-AEMP was applied during the washout of GABA and deactivation of the current after a 4-s treatment with GABA. The Fig. 5 responses to GABA alone (labeled 1) and to GABA followed immediately by 100 μM 2-AEMP (labeled 2) seemed similar, and this visual assessment was confirmed by fitting a simple exponential curve to the deactivation phase. Results obtained from the illustrated cell and from six other similarly investigated cells yielded an exponential time constant of 4.4 $\pm$ 2.0 s for the GABA-alone response and 4.7 $\pm$ 3.2 s for the response obtained with 2-AEMP present during the recovery phase. Analysis by *t* test indicated no significant difference between these values ($p > 0.05$).

Changes of 2-AEMP and TPMPA concentration made during the application of GABA indicated a substantial difference in the action of the two compounds. In Fig. 6A, wave form 1, showing the response to a 13-s application of 10 μM GABA, served as baseline for this experiment. Waveforms 2 and 3 show responses obtained, respectively, when 2-AEMP or TPMPA was-coapplied with the GABA for a 7.5-s period that began 1.5 s after the initiation of GABA presentation. The concentrations of 2-AEMP and TPMPA investigated in this experiment (18 and 7 μM, respectively) corresponded with the IC_{50} values for these compounds determined in the Fig. 4 measurements of peak amplitude. The concentrations of the two compounds being examined, although not representing a match for steady-state amplitude of the membrane current, yielded responses of mid-range decline from peak; that is, the decreases were not lost in baseline noise and they did not yield largely complete inhibition. By comparison with the response to GABA alone, the response obtained during coapplication of TPMPA (waveform 3) exhibited a progressive decrease from the peak, and conclusion of the TPMPA application led to a partial recovery of the response over the remaining period of GABA treatment The response obtained during coapplication of 2-AEMP (waveform 2) also produced a decline from the response's initial peak, and the normalized time course of this decrease closely resembled that obtained with coapplication of TPMPA (Fig. 6B). However, the cessation of inhibitor treatment produced a recovery of the response to GABA that was markedly faster and more extensive with 2-AEMP than with TPMPA. Furthermore, the cessation of 2-AEMP treatment produced a peak response amplitude that exceeded the concurrent response to GABA alone (Fig. 6A, trace 1), consistent with the reopening of the receptors by GABA upon the removal of 2-AEMP. To quantify the kinetics of inhibition release, we fitted simple exponential functions to the increasing currents exhibited on the cessation of 2-AEMP treatment. Figure 6C shows exponential time constants determined from the experiment of Fig. 6B and four other experiments of identical design. As analyzed by *t* test, the release kinetics differed significantly ($p < 0.01$); specifically, the rate of inhibition release by 2-AEMP was approximately five times as fast as that for TPMPA.

Finally, the effect of preincubating inhibitors with cells before the introduction of GABA was examined. These experiments, which used a fixed, 10-μM concentration of GABA, were designed to test the possibility that occupation of the receptor's ligand-binding site by antagonist before the introduction of GABA slows development of the GABA-induced response. Figure 7A shows results obtained in a series of experimental runs, each of which involved a 4-s application of 10 μM GABA. The black trace shows the response produced by the GABA alone, and the colored traces show the responses produced when 18 μM 2-AEMP was introduced at 0 s, 1 ms, 10 ms, 100 ms or 1 s before the application of GABA. By comparison with the GABA-alone response, the response obtained with 2-AEMP preapplication exhibited a

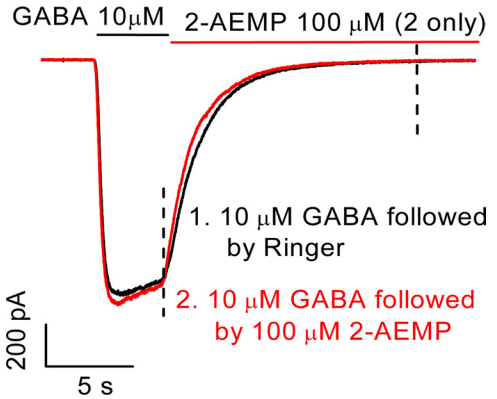

Fig. 5. Effect of presenting 2-AEMP during the deactivation phase of the GABA-induced current. Response to a 4-s application of 10 μM GABA alone (treatment 1) and to a 4-s application of 10 μM GABA followed immediately by presentation of 100 μM 2-AEMP (treatment 2). Data were obtained from a single cell.

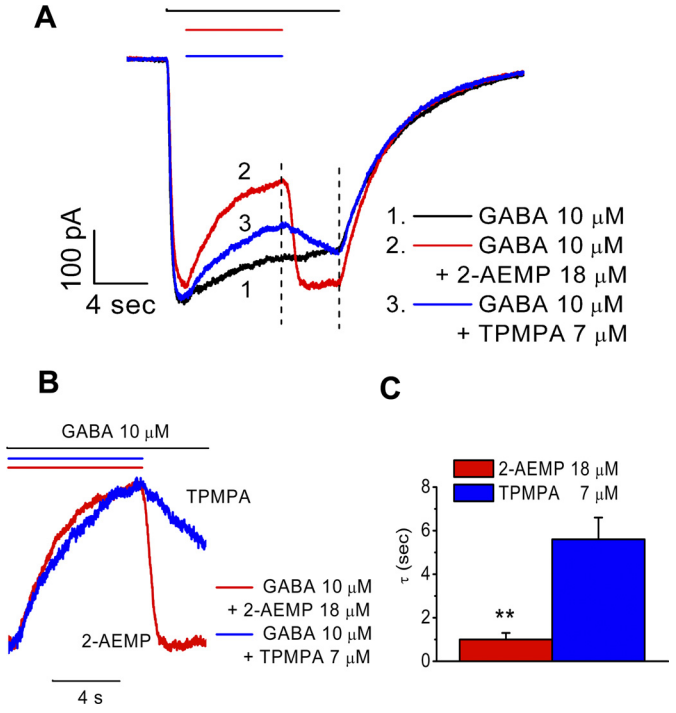

Fig. 6. Effects of 2-AEMP and of TPMPA treatment during a segment of the GABA-elicited response. A, responses to a 13-s application of 10 μM GABA alone (black stimulus marker; trace 1), and to 18 μM 2-AEMP or to 7 μM TPMPA during a 7.5-s period that began at 1.5 s after the initiation of treatment with 10 μM GABA (for 2-AEMP, red stimulus marker and trace 2; for TPMPA, blue stimulus marker and trace 3). Data obtained from a single cell. B, comparison, upon normalization, of segments of traces 2 and 3 in B. C, exponential time constants characterizing the release from inhibition of the GABA response upon the conclusion of 2-AEMP or TPMPA application. Data for 2-AEMP and TPMPA obtained, respectively, from four and seven cells.

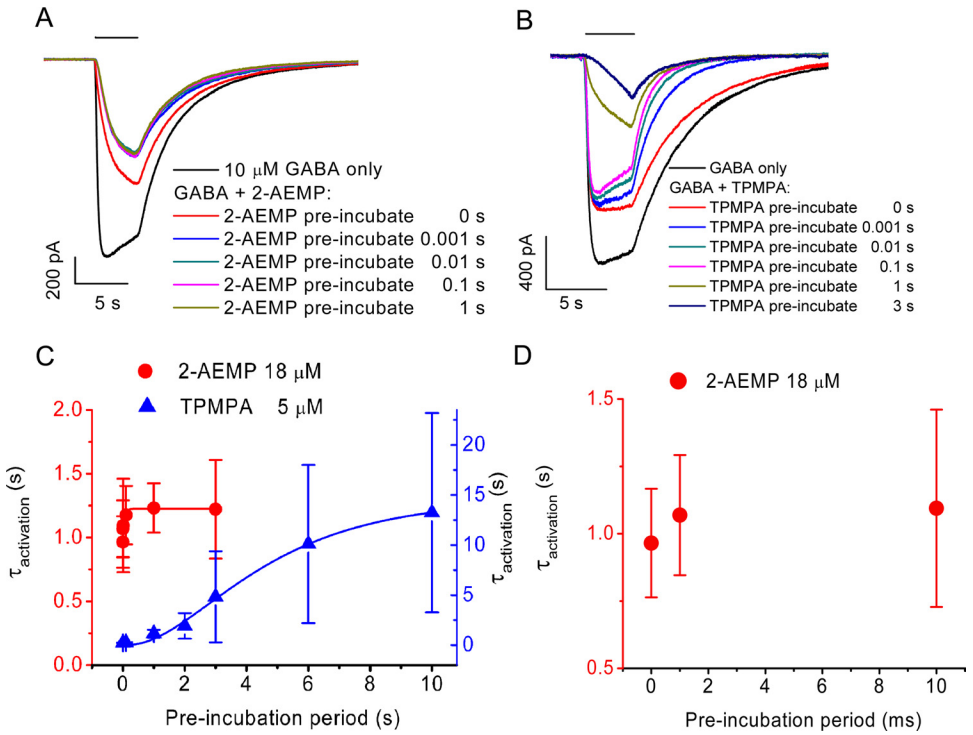

Fig. 7. Effect of preincubation with 2-AEMP and TPMPA on the GABA-elicited response. A, each of the six illustrated experimental runs involved an application of 10 μM GABA that began at $t = 0$ s and concluded at $t = 4$ s (see stimulus marker). Black trace, application of 10 μM GABA alone. Red, blue, green, purple, and yellow-green traces: applications, in addition to 10 μM GABA, of 18 μM 2-AEMP initiated, respectively, at times 0, −0.001, −0.01, −0.1 and −1 s (i.e., preincubation periods of 0, 1 ms, 10 ms, 100 ms, and 1 s, respectively). All applications of 2-AEMP concluded at $t = 4$ s. Data obtained from a single cell. B, experiment similar to that of A but with application of 5 μM TPMPA in addition to 10 μM GABA. Black trace, 4-s application of GABA alone. Red, blue, green, purple, yellow-green, and dark blue traces: application, in addition to 10 μM GABA, of TPMPA initiated at times 0, −0.001, −0.01, −0.1, −1, and −3 s, respectively. C, aggregate data obtained in four experiments involving 2-AEMP preincubation (red filled circles and red left ordinate axis) and seven experiments involving TPMPA incubation (blue filled triangles and blue right ordinate axis). Blue curve accompanying TPMPA data: eq. 4 with $\theta = 3.01$ s, $\alpha = 2.49$, A = 14.5 s, and $Y_0 = 0.112$. Red curve accompanying 2-AEMP data: eq. 4 with $\theta = 0.71$ s, $\alpha = 0.023$, A = 1.23 s, and $Y_0 = 0.00$. D, replotting, on an expanded time scale, of results obtained with brief 2-AEMP preincubations. See text for further details.

clear reduction in the rate of development of the rising phase. This decrease in rising-phase rate was evident even with a 0-s preincubation period (i.e., when the introduction of 2-AEMP coincided with the introduction of GABA). Figure 7B shows results of a similar experiment in which the application of 5 μM TPMPA was begun at defined times before GABA application. By contrast with 2-AEMP, TPMPA produced little if any reduction in rising phase rate. [Among the data obtained in four experiments of the Fig. 7B type, there seemed in some cases an increased rate of response deactivation (see Fig. 7B response obtained with 10-ms TPMPA preincubation). However, the occurrence of this change in deactivation rate was variable among experiments and among responses within an experiment. The introduction of 2-AEMP before GABA application (Fig. 7A), during GABA application (Figs. 3 and 4), or immediately after GABA application (Fig. 5) produced no substantial change in deactivation kinetics of the response. The basis of the increased deactivation rate seen in some instances with TPMPA preincubation, as in Fig. 7B, remains unclear.]

The effect of preincubation with antagonist was quantified by fitting a simple exponential function to the rising (i.e., activation) phase of the GABA-induced response and determining the time constant ($\tau_{activation}$) of this exponential function. Figure 7C summarizes the determinations of $\tau_{activation}$ in four experiments (including the experiment of Fig. 7A) that involved 2-AEMP preincubation periods of 0, 0.001, 0.01, 0.1, 1, and/or 3 s, and in seven experiments (including that of Fig. 7B) that involved TPMPA preincubation periods of 0, 0.01, and/or 1 s. Here, the determinations of $\tau_{activation}$ for 2-AEMP (red symbols) and TPMPA (blue symbols) are plotted in relation to the preincubation period; for clarity, the results obtained with 0, 1, and 10 ms preincubation periods are also shown on an expanded time scale in Fig. 7D. To characterize the time course of change in $\tau_{activation}$ with increasing period of preincubation, we analyzed the data set obtained with TPMPA through the empirically chosen equation

$$\tau_{activation} = Y_0 + A\,[1 - exp(-T/\theta)]^{\alpha} \qquad (4)$$

where T is the preincubation period, the fitted time parameter θ is a measure of the preincubation period required for near-completion of the change in $\tau_{activation}$, and Y_0, A, and α are other fitted parameters. Equation 4, which has similarities with equations used previously to analyze the onset kinetics of receptor antagonists (Jones et al., 2001), provided a close fit to the TPMPA data with $\theta_{TPMPA} = 3.01$ s (blue curve). Similar analysis of the 2-AEMP data through eq. 4 yielded $\theta_{2\text{-AEMP}} = 0.71$ s (red curve). However, by contrast with the TPMPA results, the data obtained with 2-AEMP covered only a small dynamic range. That is, values of $\tau_{activation}$ for 2-AEMP determined with the shortest preincubation periods (0, 0.001, and 0.01 s) were not substantially shorter than those determined with the longer preincubation

periods. In addition, the increase in mean value of 2-AEMP $\tau_{activation}$ over the investigated range of preincubation periods was near-complete when the preincubation period was 10 ms (Fig. 7, C and D). Based on these considerations, and on the fact that the solution exchange time for the cells is ~100 ms (see *Materials and Methods*), the Fig. 7, C and D, data provide only an upper limit, approximately 100 ms, for the characteristic time scale of the on-kinetics of 18 μM 2-AEMP.

Having characterized in detail the effects of 2-AEMP, the parent of a new class of $GABA_A$-ρ1 antagonists, in comparison with the standard $GABA_A$-ρ1 antagonist TPMPA, we performed a more basic characterization of several novel members of the class. Specifically, we prepared six new analogs of 2-AEMP (Fig. 8A) that tested the effect of substitution at each of the carbon atoms of 2-AEMP. Figure 8, B to D, shows the effects on the GABA-elicited response of four compounds similar to 2-AEMP, but possessing an additional methyl group at carbon-1 [(*R*)-**6** and (*S*)-**6**] or carbon-2 [(*R*)-**11** and (*S*)-**11**] of the 2-aminoethyl moiety. When coapplied with 10 μM GABA, the 2-(*R*)-methyl compound (*R*)-**11** produced a modest reduction in the GABA-elicited response (Fig. 8, B and C), whereas the others showed no significant inhibitory activity. However, with 1 μM GABA concentration, all of the compounds exhibited measurable antagonist activity at 100 μM concentration (Fig. 8D), with (*R*)-**11** showing the strongest inhibition as expected on the basis of the experiments conducted with 10 μM GABA. We also synthesized and tested the 2-aminoethyl esters of *n*-butylphosphonic and benzylphosphonic acid (**14** and **12**); Fig. 8, E and F). At 10 μM GABA, neither compound exhibited significant antagonist activity. As with the methylated derivatives, the activity of these compounds was evident at 1 μM GABA. However, the potency of both was far less than that of 2-AEMP. In a previous study (Chowdhury et al., 2007), no activity was observed for the benzyl compound (at 1 μM GABA) when tested in the oocyte expression system. Thus, the mammalian model system at 1 μM GABA seems to be more sensitive to antagonism than the oocyte system at 1 μM GABA. No agonist activity was observed for any of the six substituted 2-AEMP derivatives when tested at a concentration of 100 μM.

Modeling of Ligand Docking. 2-AEMP and the new phosphonic analogs studied were tested against a computational model for $GABA_A$-ρ1 antagonism. Abdel-Halim et al. (2008) used TPMPA to establish an antagonist-minimized model of the $GABA_A$-ρ1 receptor's binding pocket. In this

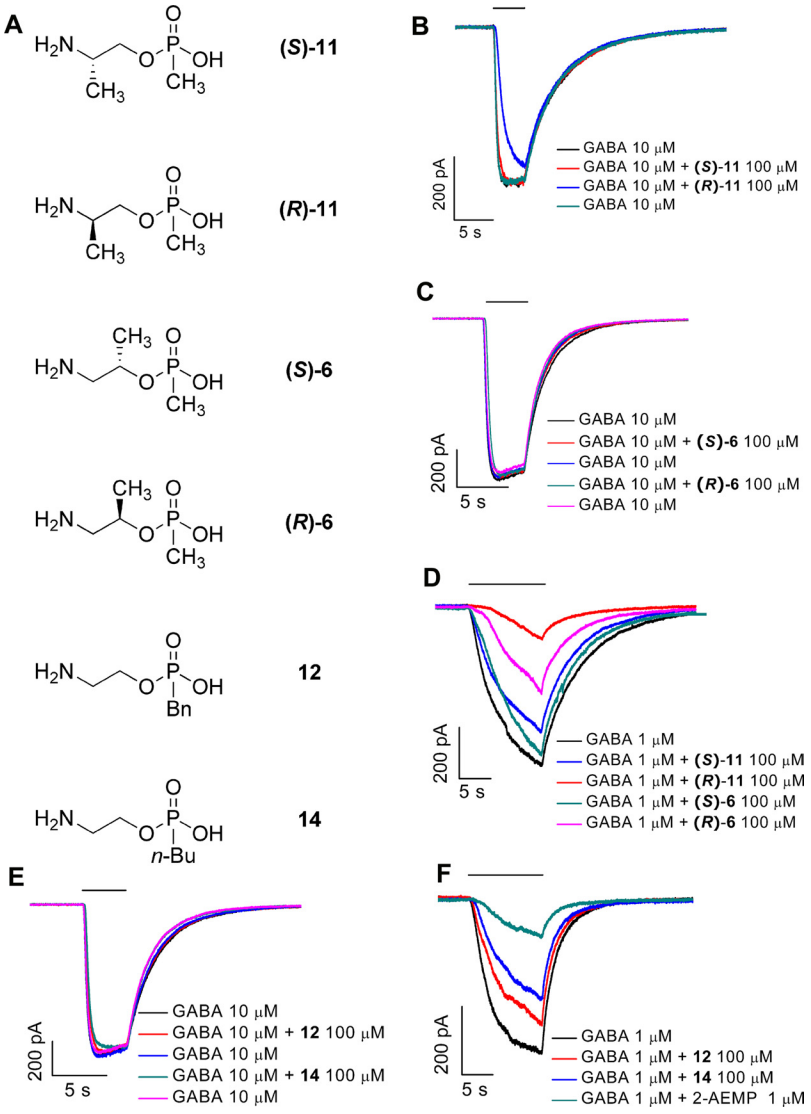

Fig. 8. Effect, on the GABA-elicited response, of compounds structurally related to 2-AEMP. A, structures of investigated compounds. B, tests of 100 μM (*R*)-**11** and 100 μM (*S*)-**11** on the response to 10 μM GABA. Here and elsewhere in this figure, the illustrated data are results obtained from a single cell; for each, top-to-bottom order in the key indicates the order of data collection. C, tests of 100 μM (*R*)-**6** and 100 μM (*S*)-**6** on the response to 10 μM GABA. D, effect of the four methyl-substituted compounds (100 μM) on the response to 1 μM GABA. E and F, tests of the benzyl analog **12** and *n*-butyl analog **14** on responses to 10 μM GABA (E) or 1 μM GABA (F).

model, the C-loop is further open by approximately 4.8 Å by comparison with an analogous agonist model obtained on minimization with GABA docking (Abdel-Halim et al., 2008). Figure 9A, reproduced from Abdel-Halim et al. (2008), illustrates the docking of TPMPA at the GABA$_A$-ρ1 ligand binding site of this antagonist model. Figure 9A may be compared with Fig. 9, B to I, which illustrate the use of this fixed-antagonist binding site configuration to dock 2-AEMP (B); 3-APMPA (C); the four methyl 2-AEMP derivatives (D–G); and the benzyl and butyl 2-AEMP analogs (H and I, respectively). Consistent with the experimental results (Fig. 8), the antagonist binding pocket accommodated 2-AEMP (B) and all of the presently investigated 2-AEMP analogs. However, docking of the benzyl analog **12** required a reduction of the van der Waals multiplier from 1.0 to 0.7, to accommodate the compound in the binding site. Furthermore, the docked orientation of the benzyl analog differed strikingly from those of the other analogs, in that the GABA-homologous region of the docked **12** was rotated and lacked several receptor interactions shared among all of the other investigated compounds. With the exception of the benzyl analog **12**, orientations of 2-AEMP and its substituted derivatives were similar to those determined for TPMPA and 3-APMPA.

The Fig. 9 modeling results specifically suggest that, with the exception of the benzyl analog **12**, the amino group of 2-AEMP and the investigated analogs, as well as these acidic oxygens attached to the phosphorus atom in these compounds, exhibit similar interactions with the receptor. Tyr198 of the receptor is a critical residue that donates a hydrogen bond through its side chain phenolic group to one of the acidic oxygen atoms, whereas its main chain carbonyl oxygen accepts a hydrogen bond from the amino group. The aromatic ring of Tyr198 can potentially form cation-π interactions with the amino group of the antagonists (Lummis et al., 2005). The other acidic oxygen atom accepts hydrogen bonds from the side chains of Ser243 and Arg104, with the latter potentially forming a salt bridge. In the case of the benzyl analog **12**, the interactions with the acidic atoms are preserved. Here, however, the interactions of the amino group of **12** with Tyr198 are absent, and the potential for a cation-π interaction is lost as a result of the lack of alignment of the amino group with the aromatic ring of Tyr198. In addition, the modeling suggests the potential for a distinctive hydrogen bond (O-O distance of 2.2–2.5Å) that connects the backbone (nonacidic) oxygen of the phosphonates with Thr244 in the binding pocket.

Discussion

The present results provide insight into the mechanism and kinetics of 2-AEMP's activity at GABA$_A$-ρ1 receptors. Consistent with the earlier brief report of data obtained from *X. laevis* oocytes (Chowdhury et al., 2007), we find that 2-AEMP acts as an antagonist at the GABA$_A$-ρ1 receptor, although with a potency less than that of 3-APMPA or TPMPA. Several types of evidence suggest that 2-AEMP acts primarily as a competitive antagonist. First, Fig. 3B shows that reducing GABA concentration diminishes the IC$_{50}$ for 2-AEMP through a parallel shift of the inhibition function. Second, from Fig. 5, it is evident that applying 2-AEMP during the GABA washout phase of the response to GABA has no significant effect on the recovery kinetics of the response. If 2-AEMP bound at a site different from GABA (i.e., noncompetitive inhibition), one might expect blockage of the current with kinetics similar to those of the onset of inhibition as shown in Fig. 7. Moreover, this absence of an effect on the deactivation kinetics cannot be explained by slow on-kinetics of 2-AEMP binding, because the time scale for the onset of inhibition by 2-AEMP (on the order of or less than 100 ms; Fig. 7, and see below) is much faster than that for receptor deactivation (4.7 s, on average; see p. 972, left column). A third type of evidence in support of a largely com-

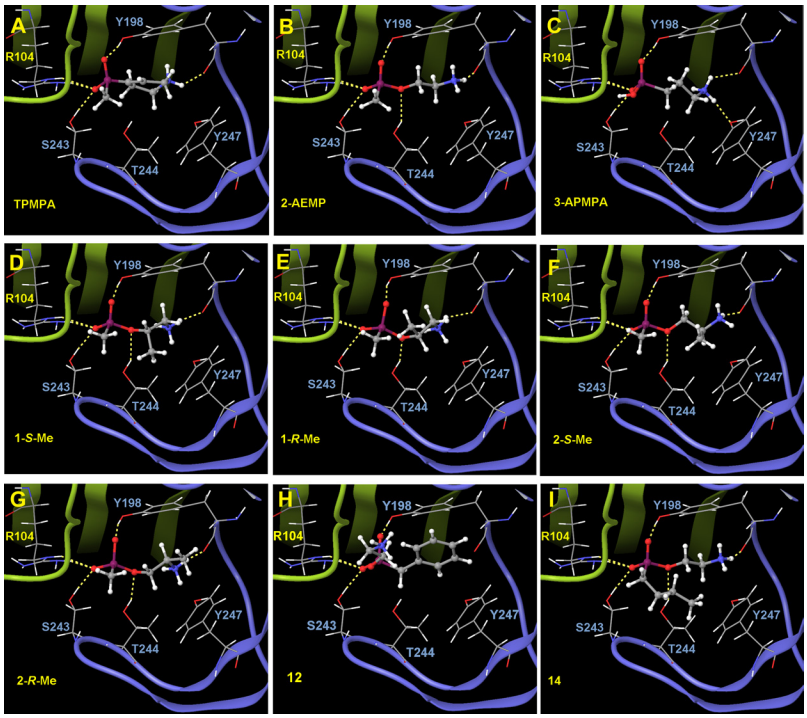

Fig. 9. Docking of compounds at the modeled antagonist binding site of the GABA$_A$-ρ1 receptor. One of several docking models obtained for each ligand is shown, and selected hydrogen bonds are depicted with dashed yellow lines. A, TPMPA; B, 2-AEMP; C, 3-APMPA. D to G, methyl analogs (*S*)-**6**, (*R*)-**6**, (*S*)-**11,** and (*R*)-**11**, respectively. H, benzyl analog **12**. I, *n*-butyl analog **14**.

petitive action of 2-AEMP comes from the binding data of Fig. 3C, which show that 2-AEMP can largely displace GABA or muscimol from $GABA_A$-ρ1-expressing cells.

The competitive antagonistic effect of 2-AEMP, in the simplest of possibilities, would be expected to produce only a rightward (i.e., desensitizing) parallel shift of the normalized GABA response function. As shown in Fig. 4D, the rightward shift was not parallel but instead exhibited a relatively sharp increase (Hill coefficient of 2.3) by contrast with the action of TPMPA. This sharpness may derive from an alteration of the receptor's gating property by 2-AEMP. For example, Wang et al. (2007), in a previous study of gating properties of $GABA_A$-ρ1 receptors in *X. laevis* oocytes, observed a similarly sharp increase in the response function obtained for the mutant E92R/R258E. These investigators determined that this change reflected an ion pair interaction in the ρ1 receptor that contributes to the gating pathway. As noted under *Results* (text accompanying Fig. 4D), 2-AEMP's antagonist activity may include a small, possibly noncompetitive component. However, it is unlikely that this noncompetitive component is substantial, in light of the evidence (Fig. 3C) that the displacement of [^{3}H]GABA and [^{3}H]muscimol by 2-AEMP was essentially complete at high 2-AEMP concentrations. On the other hand, 2-AEMP may have some activity as a blocker of the $GABA_A$-ρ1 ion channel.

A noteworthy feature of 2-AEMP's activity is that ceasing the application of 2-AEMP during the presentation of GABA increases the response amplitude to a value higher than the nominal value produced by GABA alone (Fig. 6A). This finding could derive from several possible mechanisms. For example, upon binding, 2-AEMP might render the receptor less susceptible to the gradual desensitization that ordinarily occurs with prolonged GABA application. That is, 2-AEMP might promote transition of the receptor to a fully closed state, and the removal of 2-AEMP would induce return to a relatively nondesensitized open state of the receptor. The present results furthermore show that the rate of 2-AEMP's interaction with the receptor is more rapid than that of TPMPA. Specifically, as described in Fig. 7 and the accompanying analysis involving determinations of $\tau_{activation}$, the time scale for the receptor interaction kinetics of 5 μM TPMPA is approximately 3 s, whereas that of 18 μM 2-AEMP seems to be ~100 ms or less. Although the conditions of the Fig. 7 experiments could be expected to yield an approximately 3.6-fold greater rate for 2-AEMP's onset of inhibition (because of its 3.6-fold greater concentration), this observed difference between 2-AEMP and TPMPA in the period required for the development of inhibition substantially exceeds this mass action factor.

The findings considered above suggest that 2-AEMP's inhibitory effect results largely from competition with GABA binding. However, the data leave open a number of interesting questions regarding 2-AEMP's mechanism of action. Here, an issue of possibly central importance is that the (potentially) five GABA-binding sites of the homopentameric $GABA_A$-ρ1 receptor may function differentially with respect to their interactions with GABA and 2-AEMP. These binding sites could be intrinsically different or could alter their binding properties when other sites are occupied (leading, e.g., to binding cooperativity, as suggested by the >1 Hill coefficient for the GABA dose-response function for $GABA_A$-ρ1 receptors; Amin and Weiss, 1996; Vu et al., 2005). Within this context, several of the present observations raise the intriguing possibility that, in the presence of 2-AEMP, GABA-elicited receptor activation occurs only from a mono-liganded state (i.e., only one site occupied by GABA). Previous studies have shown that $GABA_A$ receptors can open from monoliganded as well as multiliganded states (Twyman et al., 1990; Jones and Westbrook, 1995; Petrini et al., 2011). In particular, Petrini et al. (2011) have shown that monoliganded channels activate slowly and desensitize minimally by comparison with multiliganded channels. These monoliganded receptor properties are reminiscent of the behavior seen in the present study upon pre- or coapplication of 2-AEMP but not of TPMPA. Thus, is it possible that 2-AEMP occupies a subset of GABA binding sites that permits receptor activation by GABA at other sites but only in an effectively monoliganded manner. [Because full activation of $GABA_A$-ρ1 receptors is believed to require occupancy of as many as three of the five GABA-binding sites (Amin and Weiss, 1996), these considerations might, in a related manner, apply also to diliganded $GABA_A$-ρ1.] This might account for the slow activation (Fig. 4A) and protection from desensitization (Fig. 6) in the presence of 2-AEMP. Fuller correspondence with the monoliganded system described by Petrini et al. (2011) would furthermore predict relatively fast receptor deactivation in 2-AEMP, but such an increased rate of acceleration was not observed under the experimental conditions investigated here (Fig. 5).

The Fig. 8 experiments testing the physiological action of modified forms of the 2-AEMP structure show that substituents at any carbon atom reduced potency, with substitution of the pro-*R* hydrogen of C2 in the 2-aminoethyl group, affording (*R*)-**11**, the least deleterious. However, all of the compounds examined retained demonstrable antagonist activity against 1 μM GABA. In certain potential applications of these derivatives (e.g., those in which the antagonist is to be tethered directly to the receptor) (Numano et al., 2009), high potency might not be required, because tethering could be anticipated to dramatically boost the local concentration of the compound. If high potency were required of a substituted 2-AEMP derivative, the loss of potency from the substituent would need to be offset in other ways, as by conformational constraint.

The reduced potency of 2-AEMP and the methyl-substituted analogs (relative to TPMPA) is consistent with previous observations by Chebib et al. (1997), in which GABA and TACA analogs substituted with methyl or halogen at the corresponding positions were found to be less active than the parent compounds. It is noteworthy that activity is retained upon substitution with hydroxyl at carbon-3 of GABA or 3-APMPA (corresponding to carbon-1 of the 2-aminoethyl side chain in 2-AEMP) (Hinton et al., 2008), possibly because of the potential of this group to form hydrogen bonds with Thr244. The potential for hydrogen bonding at the nonacidic oxygen of 2-AEMP and derivatives could likewise be significant. Given that 2-AEMP and the other phosphonic analogs described are less potent than their phosphinic cognates, any binding energy gained through hydrogen bonding to Thr244 could partially offset deleterious changes elsewhere. Amin and Weiss (1994) have observed that residue Thr244 is important for GABA binding, and Hansen et al. (2005) have hypothesized that loop C, in which Thr244 resides, is the "induced fit 'sensor'" in the *Aplysia* acetylcholine binding protein, which is homologous to cysteine-loop receptors.

Hence, the presence of an additional hydrogen bond acceptor in the aminoethyl phosphonates versus phosphinates could contribute to the distinctive pharmacology of 2-AEMP.

The experimental results obtained with the modified 2-AEMP structures are consistent with an antagonist model of the ρ1 GABA binding site obtained with TPMPA (Fig. 10 in Abdel-Halim et al., 2008). The cavity of the antagonist model is larger than that of the agonist model obtained with minimized fitting of GABA (Abdel-Halim et al., 2008), and all but one of the substituted analogs of 2-AEMP could be docked into the antagonist model using a unit value for the van der Waals scaling of the ligand. The benzyl analog **12**, the bulkiest of the ligands and one of the weaker antagonists, could be docked only by reducing its van der Waals multiplier to 0.7. Adjustment of the van der Waals multiplier in Glide has been used previously to compensate for the possibility of induced fit by the receptor, which has a fixed geometry in the present antagonist model (Friesner et al., 2004; Halgren et al., 2004). However, even with use of a reduced van der Waals multiplier, the orientation of the docked benzyl analog differed from those of the other investigated compounds, suggesting that binding of the benzyl compound may involve a considerable reorganization of the receptor structure or exhibit an unusual binding mode. Either of these possibilities is consistent with the compound's relatively weak antagonist potency.

It is important to note that the model provides only a geometric test of the receptor's ability to accommodate compounds of interest in its binding pocket. The model is unable to establish the quantitative energetics of ligand binding or even to provide a relative ranking of binding energies. Uncertainty in the binding energy arises from several factors, not the least of which is uncertainty in the geometry of the receptor. No atomic structures of GABA receptors are known, and the receptor geometry may also vary with the number of ligands bound. Interactions of ligands with GABA receptors are known to involve cation-π interactions (Lummis et al., 2005; Padgett et al., 2007), which cannot be treated accurately with force-field (molecular mechanics) calculations. Furthermore, the rigid receptor structure of the model does not allow for induced fit to optimize receptor-ligand interactions.

Finally, the evident relative potencies of 2-AEMP and TPMPA (Fig. 4) and the relative rapidity of inhibition onset and release from inhibition by 2-AEMP (Figs. 6 and 7) raise the possibility that comparing the actions of 2-AEMP and TPMPA may be useful in future studies of GABA$_A$-ρ-mediated synaptic transmission in neural networks. It is known that low-potency, fast-acting antagonists are useful for probing the time course of glutamatergic synaptic transmission (Clements et al., 1992). Likewise, determining the response properties of GABA$_A$-ρ-expressing postsynaptic neurons under conditions of treatment with 2-AEMP versus TPMPA might represent a useful tool for distinguishing the signaling contribution specifically of locally situated postsynaptic receptors. For example, in subsecond time scale experiments involving the presentation of 2-AEMP or TPMPA to the tissue immediately before presynaptic excitation, an inhibitory effect of 2-AEMP that substantially exceeds TPMPA-induced inhibition would suggest that signal transmission at the investigated synapse is mediated largely by postsynaptic rather than extrasynaptic GABA$_A$-ρ receptors.

Acknowledgments

We thank Dr. David S. Weiss for providing the GABA$_A$-ρ1-expressing neuroblastoma cell line, Dr. Niraj J. Muni for helpful discussions, Dr. Travis R. Quick for technical assistance, and Dr. Hugh M. O'Neill for critical reading of the manuscript.

Authorship Contributions

Participated in research design: Xie, Yan, Yue, Mir, Abdel-Halim, Chebib, Le Breton, Standaert, Qian, and Pepperberg.

Conducted experiments: Xie, Yan, Yue, Feng, Mir, and Abdel-Halim.

Contributed new reagents or analytic tools: Yan and Standaert.

Performed data analysis: Xie, Yan, Yue, Mir, Abdel-Halim, Chebib, Le Breton, Standaert, Qian, and Pepperberg.

Wrote or contributed to the writing of the manuscript: Xie, Yan, Mir, Abdel-Halim, Chebib, Le Breton, Standaert, Qian, and Pepperberg.

References

Abdel-Halim H, Hanrahan JR, Hibbs DE, Johnston GA, and Chebib M (2008) A molecular basis for agonist and antagonist actions at GABA$_C$ receptors. *Chem Biol Drug Des* **71:**306–327.

Amin J and Weiss DS (1994) Homomeric ρ1 GABA channels: activation properties and domains. *Receptors Channels* **2:**227–236.

Amin J and Weiss DS (1996) Insights into the activation mechanism of ρ1 GABA receptors obtained by coexpression of wild type and activation-impaired subunits. *Proc Biol Sci* **263:**273–282.

Cates LA, Li VS, Yakshe CC, Fadeyi MO, Andree TH, Karbon EW, and Enna SJ (1984) Phosphorus analogues of γ-aminobutyric acid, a new class of anticonvulsants. *J Med Chem* **27:**654–659.

Chang Y and Weiss DS (1999) Channel opening locks agonist onto the GABA$_C$ receptor. *Nature Neurosci* **2:**219–225.

Chebib M (2004) GABA$_C$ receptor ion channels. *Clin Exp Pharmacol Physiol* **31:**800–804.

Chebib M, Hanrahan JR, Kumar RJ, Mewett KN, Morriss G, Wooller S, and Johnston GA (2007) (3-Aminocyclopentyl)methylphosphinic acids: novel GABA$_C$ receptor antagonists. *Neuropharmacology* **52:**779–787.

Chebib M, Vandenberg RJ, and Johnston GA (1997) Analogues of γ-aminobutyric acid (GABA) and *trans*-4-aminocrotonic acid (TACA) substituted in the 2 position as GABA$_C$ receptor antagonists. *Br J Pharmacol* **122:**1551–1560.

Clements JD, Lester RA, Tong G, Jahr CE, and Westbrook GL (1992) The time course of glutamate in the synaptic cleft. *Science* **258:**1498–1501.

Chowdhury S, Muni NJ, Greenwood NP, Pepperberg DR, and Standaert RF (2007) Phosphonic acid analogs of GABA through reductive dealkylation of phosphonic diesters with lithium trialkylborohydrides. *Bioorg Med Chem Lett* **17:**3745–3748.

Enz R, Brandstätter JH, Hartveit E, Wässle H, and Bormann J (1995) Expression of GABA receptor ρ1 and ρ2 subunits in the retina and brain of the rat. *Eur J Neurosci* **7:**1495–1501.

Friesner RA, Banks JL, Murphy RB, Halgren TA, Klicic JJ, Mainz DT, Repasky MP, Knoll EH, Shelley M, Perry JK, et al. (2004) Glide: a new approach for rapid, accurate docking and scoring. 1. Method and assessment of docking accuracy. *J Med Chem* **47:**1739–1749.

Friesner RA, Murphy RB, Repasky MP, Frye LL, Greenwood JR, Halgren TA, Sanschagrin PC, and Mainz DT (2006) Extra precision Glide: docking and scoring incorporating a model of hydrophobic enclosure for protein-ligand complexes. *J Med Chem* **49:**6177–6196.

Froestl W, Mickel SJ, Hall RG, von Sprecher G, Strub D, Baumann PA, Brugger F, Gentsch C, Jaekel J, Olpe HR, et al. (1995*a*) Phosphinic acid analogues of GABA. 1. New potent and selective GABA$_B$ agonists. *J Med Chem* **38:**3297–3312.

Froestl W, Mickel SJ, von Sprecher G, Diel PJ, Hall RG, Maier L, Strub D, Melillo V, Baumann PA, Bernasconi R, et al. (1995b) Phosphinic acid analogues of GABA. 2. Selective, orally active GABA$_B$ antagonists. *J Med Chem* **38:**3313–3331.

Gussin HA, Tomlinson ID, Little DM, Warnement MR, Qian H, Rosenthal SJ, and Pepperberg DR (2006) Binding of muscimol-conjugated quantum dots to GABA$_C$ receptors. *J Am Chem Soc* **128:**15701–15713.

Halgren TA, Murphy RB, Friesner RA, Beard HS, Frye LL, Pollard WT, and Banks JL (2004) Glide: A new approach for rapid, accurate docking and scoring. 2. Enrichment factors in database screening. *J Med Chem* **47:**1750–1759.

Hansen SB, Sulzenbacher G, Huxford T, Marchot P, Taylor P, and Bourne Y (2005) Structures of *Aplysia* AChBP complexes with nicotinic agonists and antagonists reveal distinctive binding interfaces and conformations. *EMBO J* **24:**3635–3646.

Harrison NJ and Lummis SC (2006) Molecular modeling of the GABA$_C$ receptor ligand-binding domain. *J Mol Model* **12:**317–324.

Hinton T, Chebib M, and Johnston GA (2008) Enantioselective actions of 4-amino-3-hydroxybutanoic acid and (3-amino-2-hydroxypropyl)methylphosphinic acid at recombinant GABA$_C$ receptors. *Bioorg Med Chem Lett* **18:**402–404.

Howson W, Mistry J, Broekman M, and Hills JM (1993) Biological-activity of (3-aminopropyl)methylphosphinic acid, a potent and selective GABA$_B$ agonist with CNS activity. *Bioorg Med Chem Lett* **3:**515–518.

Jones MV, Jonas P, Sahara Y, and Westbrook GL (2001) Microscopic kinetics and energetics distinguish GABA$_A$ receptor agonists from antagonists. *Biophys J* **81:**2660–2670.

Jones MV and Westbrook GL (1995) Desensitized states prolong $GABA_A$ channel responses to brief agonist pulses. *Neuron* **15:**181–191.
Jorgensen WL, Maxwell DS, and Tirado-Rives J (1996) Development and testing of the OPLS all-atom force field on conformational energetics and properties of organic liquids. *J Am Chem Soc* **118:**11225–11236.
Khasawneh FT, Huang JS, Mir F, Srinivasan S, Tiruppathi C, and Le Breton GC (2008) Characterization of isoprostane signaling: evidence for a unique coordination profile of 8-iso-$PGF_{2\alpha}$with the thromboxane A_2 receptor, and activation of a separate cAMP- dependent inhibitory pathway in human platelets. *Biochem Pharmacol* **75:**2301–2315.
Khasawneh FT, Huang JS, Turek JW, and Le Breton GC (2006) Differential mapping of the amino acids mediating agonist and antagonist coordination with the human thromboxane A_2 receptor protein. *J Biol Chem* **281:**26951–26965.
Krawczyk H (1997) A convenient route for monodealkylation of diethyl phosphonates. *Synth Commun* **27:**3151–3161.
Krehan D, Frølund B, Krogsgaard-Larsen P, Kehler J, Johnston GA, and Chebib M (2003) Phosphinic, phosphonic and seleninic acid bioisosteres of isonipecotic acid as novel and selective $GABA_C$ receptor antagonists. *Neurochem Int* **42:**561–565.
Lukasiewicz PD (2005) Synaptic mechanisms that shape visual signaling at the inner retina. *Prog Brain Res* **147:**205–218.
Lummis SC, Beene DL, Harrison NJ, Lester HA, and Dougherty DA (2005) A cation-π binding interaction with a tyrosine in the binding site of the $GABA_C$ receptor. *Chem Biol* **12:**993–997.
Murata Y, Woodward RM, Miledi R, and Overman LE (1996) The first selective antagonist for a $GABA_C$ receptor. *Bioorg Med Chem Lett* **6:**2073–2076.
Nehilla BJ, Popat KC, Vu TQ, Chowdhury S, Standaert RF, Pepperberg DR, and Desai TA (2004) Neurotransmitter analog tethered to a silicon platform for neuro-BioMEMS applications. *Biotechnol Bioeng* **87:**669–674.
Numano R, Szobota S, Lau AY, Gorostiza P, Volgraf M, Roux B, Trauner D, and Isacoff EY (2009) Nanosculpting reversed wavelength sensitivity into a photoswitchable iGluR. *Proc Natl Acad Sci USA* **106:**6814–6819.
Olsen RW and Sieghart W (2009) $GABA_A$ receptors: subtypes provide diversity of function and pharmacology. *Neuropharmacology* **56:**141–148.
Padgett CL, Hanek AP, Lester HA, Dougherty DA, and Lummis SC (2007) Unnatural amino acid mutagenesis of the $GABA_A$ receptor binding site residues reveals a novel cation-π interaction between GABA and β_2Tyr97. *J Neurosci* **27:**886–892.
Petrini EM, Nieus T, Ravasenga T, Succol F, Guazzi S, Benfenati F, and Barberis A (2011) Influence of $GABA_A$R monoliganded states on GABAergic responses. *J Neurosci* **31:**1752–1761.
Qian H and Dowling JE (1993) Novel GABA responses from rod-driven retinal horizontal cells. *Nature* **361:**162–164.
Ragozzino D, Woodward RM, Murata Y, Eusebi F, Overman LE, and Miledi R (1996) Design and in vitro pharmacology of a selective γ-aminobutyric $acid_C$ antagonist. *Mol Pharmacol* **50:**1024–1030.
Saifuddin U, Vu TQ, Rezac M, Qian H, Pepperberg DR, and Desai TA (2003) Assembly and characterization of biofunctional neurotransmitter-immobilized surfaces for interaction with postsynaptic membrane receptors. *J Biomed Mater Res A* **66:**184–191.
Sedelnikova A, Smith CD, Zakharkin SO, Davis D, Weiss DS, and Chang Y (2005) Mapping the ρ_1 $GABA_C$ receptor agonist binding pocket. Constructing a complete model. *J Biol Chem* **280:**1535–1542.
Song XQ, Meng F, Ramsey DJ, Ripps H, and Qian H (2005) The GABA ρ1 subunit interacts with a cellular retinoic acid binding protein in mammalian retina. *Neuroscience* **136:**467–475.
Torres VI and Weiss DS (2002) Identification of a tyrosine in the agonist binding site of the homomeric ρ1 γ-aminobutyric acid (GABA) receptor that, when mutated, produces spontaneous opening. *J Biol Chem* **277:**43741–43748.
Twyman RE, Rogers CJ, and Macdonald RL (1990) Intraburst kinetic properties of the $GABA_A$ receptor main conductance state of mouse spinal cord neurones in culture. *J Physiol* **423:**193–220.
Volgraf M, Gorostiza P, Numano R, Kramer RH, Isacoff EY, and Trauner D (2006) Allosteric control of an ionotropic glutamate receptor with an optical switch. *Nat Chem Biol* **2:**47–52.
Vu TQ, Chowdhury S, Muni NJ, Qian H, Standaert RF, and Pepperberg DR (2005) Activation of membrane receptors by a neurotransmitter conjugate designed for surface attachment. *Biomaterials* **26:**1895–1903.
Wang J, Lester HA, and Dougherty DA (2007) Establishing an ion pair interaction in the homomeric ρ1 γ-aminobutyric acid type A receptor that contributes to the gating pathway. *J Biol Chem* **282:**26210–26216.
Xie A, Feng F, Yan J, Standaert RF, Pepperberg DR, and Qian H (2009) Comparison of inhibitory mechanism for 2-aminoethyl methylphosphonate (2-AEMP) and TPMPA at $GABA_C$ receptors. 2009 Annual Meeting of the Association for Research in Vision and Ophthalmology (ARVO). *Invest Ophthalmol Vis Sci* **50:**1016A.
Xie A, Yue L, Feng F, Mir F, Yan J, Welsh LM, Wang J, Frishman LJ, Kaplan JH, Standaert RF, et al. (2008) 2-aminoethyl methylphosphonate analog of GABA: antagonist activity at $GABA_C$ receptors. *Soc Neurosci Abstr* **34:**608.10.

Address correspondence to: Dr. David R. Pepperberg, Department of Ophthalmology and Visual Sciences, University of Illinois at Chicago, 1855 West Taylor Street, Chicago, IL 60612. E-mail: davipepp@uic.edu